NUDIX Hydrolases Target Specific Inositol Pyrophosphates and Regulate Phosphate and Iron Homeostasis, and the Expression of Defense Genes in Arabidopsis

Robin Schneider[1§], Klea Lami[1§], Isabel Prucker[2§], Sara Christina Stolze[3], Annett Strauß[4], Kevin Langenbach[1], Marília Kamleitner[1], Yemisrach Zewdu Belay[1], Kevin Ritter[2], David Furkert[6], Philipp Gaugler[1], Esther Lange[1], Natalie Faiß[4], Julie Marie Schmidt[1], Michael Harings[1], Lukas Krusenbaum[1], Stefanie Wege[1], Simon Kriescher[1] Jeremy The[5], Heiko Schoof[5], Dorothea Fiedler[6], Hirofumi Nakagami[3], Ricardo F. H. Giehl[7], Thomas Lahaye[4], Henning J. Jessen[2], Verena Gaugler[1]*, Gabriel Schaaf[1]*

[1]Department of Plant Nutrition, Institute of Crop Science and Resource Conservation, Rheinische Friedrich-Wilhelms-Universität Bonn, 53115 Bonn, Germany

[2]Department of Chemistry and Pharmacy and CIBSS-Centre for Integrative Biological Signalling Studies, Albert-Ludwigs University Freiburg, 79104 Freiburg, Germany

[3]Protein Mass Spectronomy, Max Planck Institute for Plant Breeding Research, 50829 Cologne, Germany

[4]Department of General Genetics, Center of Plant Molecular Biology (ZMBP) University of Tübingen, 72076 Tübingen, Germany

[5]Department of Crop Bioinformatics, Institute of Crop Science and Resource Conservation, Rheinische Friedrich-Wilhelms-Universität Bonn, 53115 Bonn, Germany

[6]Leibniz-Forschungsinstitut für Molekulare Pharmakologie (FMP), 13125 Berlin, Germany

[7]Department of Physiology & Cell Biology, Leibniz-Institute of Plant Genetics and Crop Plant Research, 06466 Gatersleben (IPK), Germany

[§] R.S., Kl.L. and I.P. contributed equally to this manuscript.

*E-mail: gabriel.schaaf@uni-bonn.de, verena.gaugler@uni-bonn.de

ORCID: R.S. 0000-0002-9657-4548, Kl.L. 0009-0000-6750-1350, I.P. 0000-0002-5794-6759, S.C.S. 0000-0002-1421-9703, A.S. 0000-0002-2266-6239, Ke.L. 0009-0008-4271-1034, M.K. 0000-0002-8598-2423, Y.Z.B. 0009-0006-8320-7032, K.R. 0000-0001-7900-1855, Da.F. 0000-0002-6145-5397, P.G. 0000-0002-9187-404X, E.L. 0000-0001-8097-8997, N.F. 0009-0000-1893-6462, J.M.S. 0009-0008-6783-0814, M.H. 0009-0007-1065-818X, L.K. 0000-0001-

5519-2765, S.W. 0000-0002-7232-5889, S.K. 0009-0003-7132-1899, J.T. 0009-0005-4817-0847, H.S. 0000-0002-1527-3752, Do.F. 0000-0002-0798-946X, H.N. 0000-0003-2569-7062, R.F.H.G. 0000-0003-1006-3163, T.L. 0000-0001-5257-336X, H.J.J: 0000-0002-1025-9484, V.G. 0000-0002-3249-2922, G.S. 0000-0001-9022-4515

Abstract

Inositol pyrophosphates (PP-InsPs) are important signaling molecules that regulate diverse cellular processes in eukaryotes, including energy homeostasis and phosphate (P_i) signaling. However, the enzymes responsible for their turnover in plants remain largely unknown. Using a non-hydrolysable PP-InsP analog in a pull-down approach, we identified a family of Arabidopsis Nudix hydrolases (NUDTs) that group into two closely related subclades. Through *in vitro* assays, heterologous expression systems, and higher-order gene-edited mutants, we explored the substrate specificities and physiological roles of these hydrolases. Using a combination of strong anion exchange (SAX)-HPLC, PAGE, and capillary electrophoresis electrospray ionization mass spectrometry (CE-ESI-MS), we found that their PP-InsP pyrophosphatase activity is enantiomer-selective and Mg^{2+}-dependent. Specifically, subclade I NUDTs preferentially hydrolyze 4-$InsP_7$, while subclade II NUDTs target 3-$InsP_7$, with minor activity against other PP-InsPs, including 5-$InsP_7$. In higher-order mutants of subclade II NUDTs, we observed defects in both P_i and iron homeostasis, accompanied by increased levels of 1/3-$InsP_7$ and 5-$InsP_7$, with a markedly larger increase in 1/3-$InsP_7$. Furthermore, ectopic expression of NUDTs from both subclades induced local P_i starvation responses (PSRs). However, RNA-seq analysis of WT and *nudt12/13/16* plants suggests that these NUDTs have PSR-independent roles, potentially involving 1/3-$InsP_7$ in the regulation of plant defense. Expanding beyond subclade II NUDTs, we demonstrated susceptibility of the 3PP-position of PP-InsPs to enzymatic activities unrelated to NUDTs, and found that such activities are conserved across plants and humans. Additionally, we found that NUDT effectors from pathogenic ascomycete fungi exhibit a substrate specificity similar to subclade I NUDTs. Collectively, our study provides new insights into the roles of NUDTs in regulating PP-InsP signaling pathways in plants and highlights cross-kingdom conservation of enzymes involved in PP-InsP metabolism.

Introduction

Inositol pyrophosphates (PP-InsPs) are small signaling molecules consisting of a phosphorylated *myo*-inositol ring and one or several pyrophosphate groups, which regulate a wide range of cellular processes in eukaryotes. In metazoans, these messengers control DNA repair, insulin signaling, blood clotting, ribosome biogenesis, spermiogenesis, and telomere length maintenance (Stephens *et al.*, 1993; Menniti *et al.*, 1993; Shears, 2015, 2018; Thota & Bhandari, 2015). In plants, PP-InsPs regulate jasmonate and auxin signaling, as well as a nutrient status-dependent accumulation of storage lipids (Laha *et al.*, 2015, 2016, 2022; Couso *et al.*, 2016). An emerging and somewhat unifying role of these messengers in fungi, metazoans and plants is their critical involvement in energy homeostasis and phosphate (P_i) signaling (Lee *et al.*, 2007; Szijgyarto *et al.*, 2011; Wild *et al.*, 2016; Dong *et al.*, 2019; Wilson *et al.*, 2019; Zhu *et al.*, 2019; Li *et al.*, 2020; Ried *et al.*, 2021; Wang *et al.*, 2021; Riemer *et al.*, 2021; Gulabani *et al.*, 2022; Qin *et al.*, 2023; Chabert *et al.*, 2023).

Phosphorus (P) is an essential macronutrient and a key determinant of agricultural yield (Tilman *et al.*, 2002; MacDonald *et al.*, 2011; Hawkesford *et al.*, 2023). Plants have evolved complex sensing and signaling mechanisms to adjust the plant's P demand with external P_i availability. In Arabidopsis, the MYB transcription factors PHR1 and PHL1 regulate the expression of P_i starvation-induced (PSI) genes (Rubio *et al.*, 2001; Bustos *et al.*, 2010). Under P_i deficiency, PHR1 activates PSI genes by binding to cognate binding elements (P1BS) in their promoter region. Under P_i sufficiency, stand-alone SPX proteins negatively regulate PHR transcription factors, as shown in various plant species (Liu *et al.*, 2010; Shi *et al.*, 2014; Lv *et al.*, 2014; Puga *et al.*, 2014; Wang *et al.*, 2014; Qi *et al.*, 2017; Zhong *et al.*, 2018; Osorio *et al.*, 2019; Ried *et al.*, 2021). Intriguingly, SPX proteins function as cellular receptors for certain PP-InsPs such as 5-$InsP_7$ and $InsP_8$ (Wild *et al.*, 2016; Gerasimaite *et al.*, 2017; Dong *et al.*, 2019; Zhu *et al.*, 2019; Li *et al.*, 2020; Pipercevic *et al.*, 2023; Yan *et al.*, 2024). When bound to $InsP_8$, SPX proteins interact with the unique coiled-coil motif of PHR1, interfering with its oligomerization and promoter-binding activity (Ried *et al.*, 2021). Consequently, mutants defective in these PP-InsPs display constitutively up-regulated P_i starvation responses (PSRs) both locally and systemically, suggesting that plants are largely unable to sense P_i directly but sense certain PP-InsPs as a proxy for P_i (Dong *et al.*, 2019; Zhu *et al.*, 2019; Riemer *et al.*, 2021). Likewise, disruptions of lower InsP kinases like IPK2alpha, IPK2beta and IPK1 also result in reduction of PP-InsPs and impaired phosphate homeostasis (Stevenson-Paulik *et al.*, 2002, 2005; Kuo *et al.*, 2014, 2018; Riemer *et al.*, 2021). However, the regulation of these PSRs and the precise mechanisms and regulation of P_i sensing in plants still remains poorly understood.

The analysis of PP-InsPs, as well as simple inositol polyphosphates (InsPs) that lack the pyrophosphate moiety, remains challenging due to their high charge density and, in the case of many isomers, low abundance. Various technological advances, including strong anion exchange (SAX)-HPLC of [^{3}H] *myo*-inositol-labeled cell extracts (Lemtiri-Chlieh *et al.*, 2000; Flores & Smart, 2000; Laha *et al.*, 2015; Gaugler *et al.*, 2020), as well as titanium dioxide (TiO_2)-based purification of InsPs/PP-InsPs followed by polyacrylamide gel electrophoresis (PAGE) separation and visualization with toluidine blue/DAPI, have been instrumental in identifying and characterizing these messengers in many eukaryotes, including plants (Losito *et al.*, 2009; Wilson *et al.*, 2015). However, these methods fail to separate PP-InsP isomers of identical molecular mass. A major breakthrough was the development of capillary electrophoresis electrospray ionization mass spectrometry (CE-ESI-MS) (Qiu *et al.*, 2020), which allowed the identification of three major $InsP_7$ (sometimes referred to as PP-$InsP_5$) isomers in plant extracts: 1-$InsP_7$ (carrying the PP-moiety at the 1-position) and/or 3-$InsP_7$ (hereafter referred to as 1/3-$InsP_7$), 4-$InsP_7$ and/or 6-$InsP_7$ (hereafter referred to as 4/6-$InsP_7$), and 5-$InsP_7$ (Riemer *et al.*, 2021). Because $InsP_6$, like *myo*-inositol, is a *meso* compound with a plane of symmetry dissecting the 2 and 5 positions, the 1/3 and 4/6 phosphates are enantiomeric and cannot be distinguished in the absence of chiral selectors (Blüher *et al.*, 2017; Ritter *et al.*, 2023) (Figure S1). In addition, CE-ESI-MS allowed identification of a novel PP-$InsP_4$ isomer of unknown isomer identity in Arabidopsis roots (Riemer *et al.*, 2021).

The biosynthetic pathways of PP-InsPs are only partially resolved. All eukaryotes appear to possess 5-$InsP_7$, but its synthesis from phytate ($InsP_6$) is mediated by distinct, sequence-unrelated enzyme families. In budding yeast (*Saccharomyces cerevisiae*) and mammals, the phosphorylation of $InsP_6$ to 5-$InsP_7$ is catalyzed by Kcs1/IP6K-type kinases (Saiardi *et al.*, 1999; Draškovič *et al.*, 2008), a protein family absent in higher plants (Laha *et al.*, 2015, 2019). In contrast, plant 5-$InsP_7$ synthesis is catalyzed by inositol (1,3,4) trisphosphate 5/6-kinases (ITPKs), as shown *in vitro* and yeast for various Arabidopsis and rice ITPKs (Laha *et al.*, 2019; Whitfield *et al.*, 2020), and as shown *in planta* for AtITPK1 and AtITPK2 (Riemer *et al.*, 2021; Laha *et al.*, 2022).

The synthesis of $InsP_8$ from 5-$InsP_7$ appears to be largely conserved in eukaryotes and is catalyzed by members of a protein family distinct from the above mentioned $InsP_6$ kinases. In budding yeast and mammals, these enzymes were named Vip1 and PPIP5K-type kinases, respectively (Mulugu *et al.*, 2007; Lin *et al.*, 2009; Wang *et al.*, 2011). In Arabidopsis, the synthesis of $InsP_8$ is catalyzed by two PPIP5K isoforms, namely AtVIH1 and AtVIH2 (Desai *et al.*, 2014; Laha *et al.*, 2015; Dong *et al.*, 2019; Zhu *et al.*, 2019). With the exception of the budding yeast PPIP5K Vip1 and the human PPIP5K2, both of which specifically generate 1-$InsP_7$ and 1,5-$InsP_8$ (Mulugu *et al.*, 2007; Fridy *et al.*, 2007; Dollins *et al.*, 2020), it remains

unclear whether other PPIP5K isoforms catalyze the formation of the phosphoanhydride bond at the 1 or the 3 position of the fully phosphorylated *myo*-inositol ring. Therefore, the enantiomer identities of 1/3-$InsP_7$ and 1/3,5-$InsP_8$ in mammals and plants are still unknown. Besides, our knowledge about PP-InsP turnover in plants remains incomplete. Similar to yeast and mammalian PPIP5Ks, AtVIH1 and AtVIH2 are bifunctional enzymes, harboring an N-terminal ATP-grasp kinase domain and a C-terminal phosphatase-like domain (Mulugu *et al.*, 2007; Fridy *et al.*, 2007; Wang *et al.*, 2011; Laha *et al.*, 2015; Zhu *et al.*, 2019). *In vitro*, the latter has been shown to hydrolyze 1-$InsP_7$, and 5-$InsP_7$ to $InsP_6$ for Arabidopsis VIH2, and 1-$InsP_7$ and 1,5-$InsP_8$ to $InsP_6$ and 5-$InsP_7$, respectively, for the fission yeast PPIP5K homolog Asp1 and for yeast Vip1 (Wang *et al.*, 2015; Pascual-Ortiz *et al.*, 2018; Zhu *et al.*, 2019; Dollins *et al.*, 2020). At low adenylate energy charge, AtITPK1 can catalyze a reverse reaction, transferring the β-phosphate from 5-$InsP_7$ to ADP to generate $InsP_6$ and ATP, presumably as a quick and energy-saving mechanism to shut down phosphate starvation responses (Whitfield *et al.*, 2020; Riemer *et al.*, 2021). Recently, also specific inositol phosphohydrolases, namely the *Arabidopsis thaliana* Plant and Fungi Atypical Dual Specificity Phosphatases (PFA-DSP1-5), were identified in plants. Similarly to the activity of the budding yeast homologue Siw14 (Steidle *et al.*, 2016; Wang *et al.*, 2018), all five PFA-DSP isoforms displayed robust and highly specific pyrophosphatase activities towards the 5-β-phosphates of 5-$InsP_7$ and 1/3,5-$InsP_8$ (Wang *et al.*, 2022; Gaugler *et al.*, 2022). However, the enzymes involved in the hydrolysis of other $InsP_7$ isomers, such as 1-$InsP_7$ and/or 3-$InsP_7$, as well as 4-$InsP_7$ and/or 6-$InsP_7$, remain unknown in plants. The identification of the respective PP-InsP pyrophosphatases will therefore provide a helpful tool to identify the physiological roles of these messengers.

To this end, we took advantage of a non-hydrolysable $InsP_7$ analog, 5PCP-$InsP_5$ (Wu *et al.*, 2016), in which the oxygen of a phosphoanhydride bond is substituted by a carbon, to carry out affinity pull-down experiments and identified Arabidopsis NUDIX proteins as potential interactors of $InsP_7$. NUDIX is an acronym for 'NUcleoside DIphosphate linked to some other moiety X,' reflecting the diverse nucleoside diphosphate substrates targeted by NUDIX-type (NUDT) hydrolases. The budding yeast ScDdp1 (Safrany *et al.*, 1999; Lonetti *et al.*, 2011; Andreeva *et al.*, 2019) and the five human hsDIPP proteins (DIPP1, 2α, 2β, 3α and 3β) (Kilari *et al.*, 2013) are members of the NUDIX family and were shown to hydrolyze preferentially the β-phosphate of 1-$InsP_7$. We provide evidence that members of two different subclades of these phosphohydrolases display distinct and highly specific PP-InsP pyrophosphatase activities. Subclade I members NUDT4, NUDT17, NUDT18 and NUDT21 show a preference for the 4-pyrophosphate moiety and subclade II members NUDT12, NUDT13 and NUDT16 show a preference for the 3-pyrophosphate moiety of PP-InsPs. We demonstrate that subclade II

members play a role in P_i and iron (Fe) homeostasis, regulate defense gene expression, and that the 3PP-position of PP-InsPs is a preferred substrate for conserved enzymatic activities unrelated to NUDTs.

Results

Pull-down of *Arabidopsis thaliana* NUDT hydrolases with a non-hydrolysable $InsP_7$ analog

In an attempt to identify potential PP-InsP interactors, we performed an affinity pull-down assay using 5PCP-$InsP_5$ beads, a reagent consisting of a non-hydrolysable $InsP_7$ analog coupled to a solid phase resin (Wu *et al.*, 2016; Furkert *et al.*, 2021), which were incubated with Arabidopsis shoot or root extracts. Bound proteins were eluted with a high molar excess of $InsP_6$, and both beads and eluates were trypsinized and resulting peptides analyzed separately for eluate and on-bead fractions by liquid chromatography–mass spectrometry (LC-MS/MS) to identify proteins interacting with $InsP_7$. The peptide analysis revealed known proteins involved in InsP/PP-InsP metabolism such as MIPS3 (Luo *et al.*, 2011; Fleet *et al.*, 2018), IPK2alpha and IPK2beta (Stevenson-Paulik *et al.*, 2002, 2005; Xia *et al.*, 2003), ITPK3 (Sweetman *et al.*, 2007), VIH1, VIH2, $InsP_6$/PP-InsP-binding proteins such as the jasmonate co-receptor F-box protein COI1, various TIR1/COI1 homologs (AFB1, AFB2, AFB3), components of the TIR1/COI1-dependent SKP1-CUL1-F-box protein (SCF) ubiquitin E3 ligase complex (ASK1, ASK2, CUL1, CUL2), as well as the presumed $InsP_8$ binding protein SPX2 (Ried et al. 2021) (Table S1). Besides these known $InsP_6$/PP-InsP binding proteins or enzymes involved in InsP/PP-InsP metabolism, peptides of five different NUDT hydrolases were identified in shoot and root extracts. Three of these, NUDT4, NUDT17 and NUDT21 were present in eluates or beads incubated with Arabidopsis shoot extracts, while two, NUDT16 and NUDT18, were detected in root extracts (Table S1). The identified NUDT hydrolases are closely related and can be grouped into a clade in the phylogenetic tree of the 29 Arabidopsis NUDT hydrolases, in which two additional members, namely NUDT12 and -13, are also included (Figure 1A). The clade can be divided into two subclades, with NUDT4, -17, -18, and -21 designated as subclade I and NUDT12, -13, and -16 designated as subclade II. The physiological role of these hydrolases and their substrates *in planta* remain unknown. We therefore decided to investigate all seven NUDT hydrolases of the clade for their possible involvement in inositol pyrophosphate metabolism, including those that were not isolated with the affinity pull-down assay.

Heterologous expression of Arabidopsis subclade I and II NUDTs partially complement yeast *ddp1Δ* defects

Considering that NUDTs share homology with yeast Ddp1 and mammalian DIPP proteins, all of which display pyrophosphatase activity against 1-$InsP_7$, we investigated whether the heterologous expression of subclade I and II NUDTs rescues the metabolic defects of the yeast *ddp1Δ* mutant. This yeast mutant strongly accumulates 1-$InsP_7$ as compared to its isogenic WT strain (Lonetti *et al.*, 2011)(Figure 1B and C). As revealed by SAX-HPLC analyses of extracts from [^{3}H] *myo*-inositol-labeled yeast transformants, we observed that, with the exception of NUDT4 and NUDT18, expression of all subclade I and II NUDTs partially rescued the *ddp1Δ*-associated defects in $InsP_7$ degradation (Figure 1B and C). Because plants likely possess at least one form of 4/6-$InsP_7$ and one form of 1/3-$InsP_7$, although the respective enantiomer identities remain unresolved, and since yeast lacks 4/6-$InsP_7$ and 3-$InsP_7$, we resorted to *in vitro* assays to further investigate the substrate specificities of subclade I and II NUDTs.

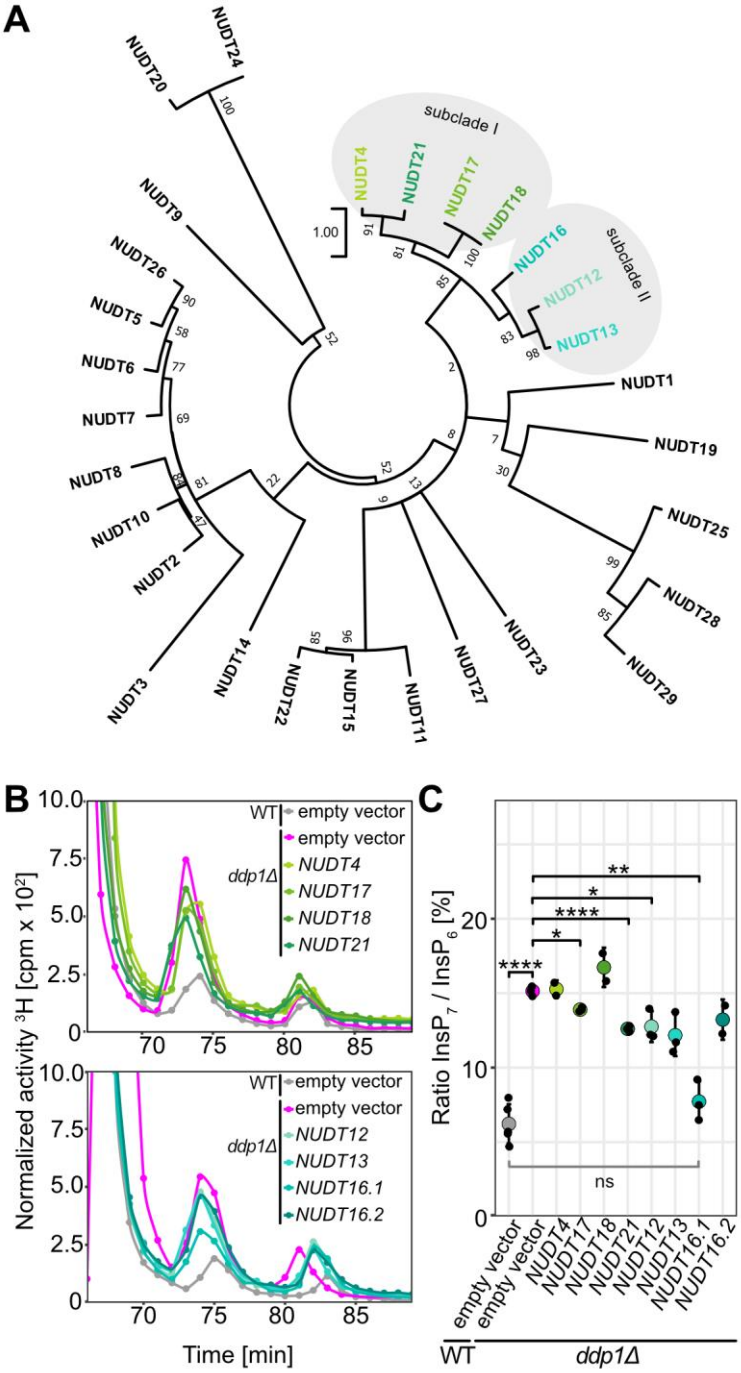

Figure 1: Identified Arabidopsis NUDT hydrolases group in two subclades and heterologous expression partially complements *ddp1Δ*-associated defects in $InsP_7$ levels in yeast. Phylogenetic tree of 29 Arabidopsis NUDT hydrolases (A). The tree was created with MEGA11 and the Jones-Taylor-Thornton method with 500 bootstrap replications. Arabidopsis NUDT4, -17, -18, and -21 can be grouped as a subclade of the phylogenetic tree (subclade I). NUDT12, -13, and -16 can also be grouped as a subclade (subclade II) and together with subclade I as one clade in the phylogenetic tree. (B) SAX-HPLC profiles of radiolabeled *ddp1Δ* yeast transformed with either empty vector (pAG425GPD-*ccdB*), or pAG425GPD carrying the respective *NUDT* gene. Depicted are representative SAX-HPLC runs of one experiment. The experiment was repeated with similar results (n = 3 or 4, except for NUDT4, NUDT18, NUDT16.2, n = 2). Combined data are shown in Figure 1B. (C) Relative amounts of $InsP_7$ of wild-type and *ddp1Δ* yeast transformed with empty vector, and *ddp1Δ* transformed with pAG425GPD carrying the *NUDT* genes are shown as $InsP_7/InsP_6$ ratios. $InsP_6$ and $InsP_7$ levels

were determined by SAX-HPLC analyses and data were processed with R. Data represents mean ± SD. Asterisks indicate values that are are significantly different from *ddp1Δ* according to Student's *t* test ($P < 0.05$ (*); $P < 0.01$ (**); $P < 0.001$ (***); $P < 0.0001$ (****)).

In vitro biochemical analyses reveal distinct and highly specific PP-InsP pyrophosphatase activities for Arabidopsis subclade I and II NUDT proteins

We took advantage of chemically synthesized enantiomerically pure $InsP_7$ and $InsP_8$ isomers for more thorough biochemical analyses (Capolicchio *et al.*, 2013, 2014). To this end, we generated recombinant NUDTs, N-terminally fused with a hexahistidine (His_6) maltose-binding protein (MBP) tag. A His-tag-MBP protein served as a negative control. *In vitro* reactions with $InsP_6$ or different $InsP_7$ isomers were performed in the presence of Mg^{2+}. By separating the reaction via PAGE, we observed nearly complete hydrolysis of 4-$InsP_7$ in presence of subclade I hydrolases (NUDT4, NUDT17, NUDT18 or NUDT21) (Figure 2A). The hydrolysis product showed the same mobility as $InsP_6$ on PAGE (Figure 2A), and CE-ESI-MS measurements of reactions spiked with [$^{13}C_6$] $InsP_6$ standards also confirmed that the product had the same migration time and mass as $InsP_6$ (Figure S3). Consequently, a significant increase of $InsP_6$ from 4-$InsP_7$ was observed in reactions with subclade I NUDT hydrolases compared to the negative control, as determined by CE-ESI-MS analyses (Figure 2B). Notably, there was also a robust hydrolysis of 6-$InsP_7$ in the presence of NUDT18 (Figure 2A and B) with minor activities of NUDT4 against 1-$InsP_7$ and of NUDT21 against 3-$InsP_7$ (Figure 2A and B). In contrast, under these conditions, none of the subclade I NUDTs was able to hydrolyze $InsP_6$ or 5-$InsP_7$ *in vitro* (Figure 2A and B and Figure S2).

We also tested whether subclade I NUDTs can catalyze the hydrolysis of 4-$InsP_7$ in the presence of alternative divalent cations, such as Ca^{2+}, Zn^{2+}, Mn^{2+} or in the absence of any divalent cations by using the metal chelator EDTA. In all reactions where Mg^{2+} was absent and either alternative cofactors or EDTA were present, no 4-$InsP_7$ hydrolysis was observed, revealing the critical role of Mg^{2+} as a cofactor for NUDT subclade I-dependent 4-$InsP_7$ hydrolysis (Figure 2C).

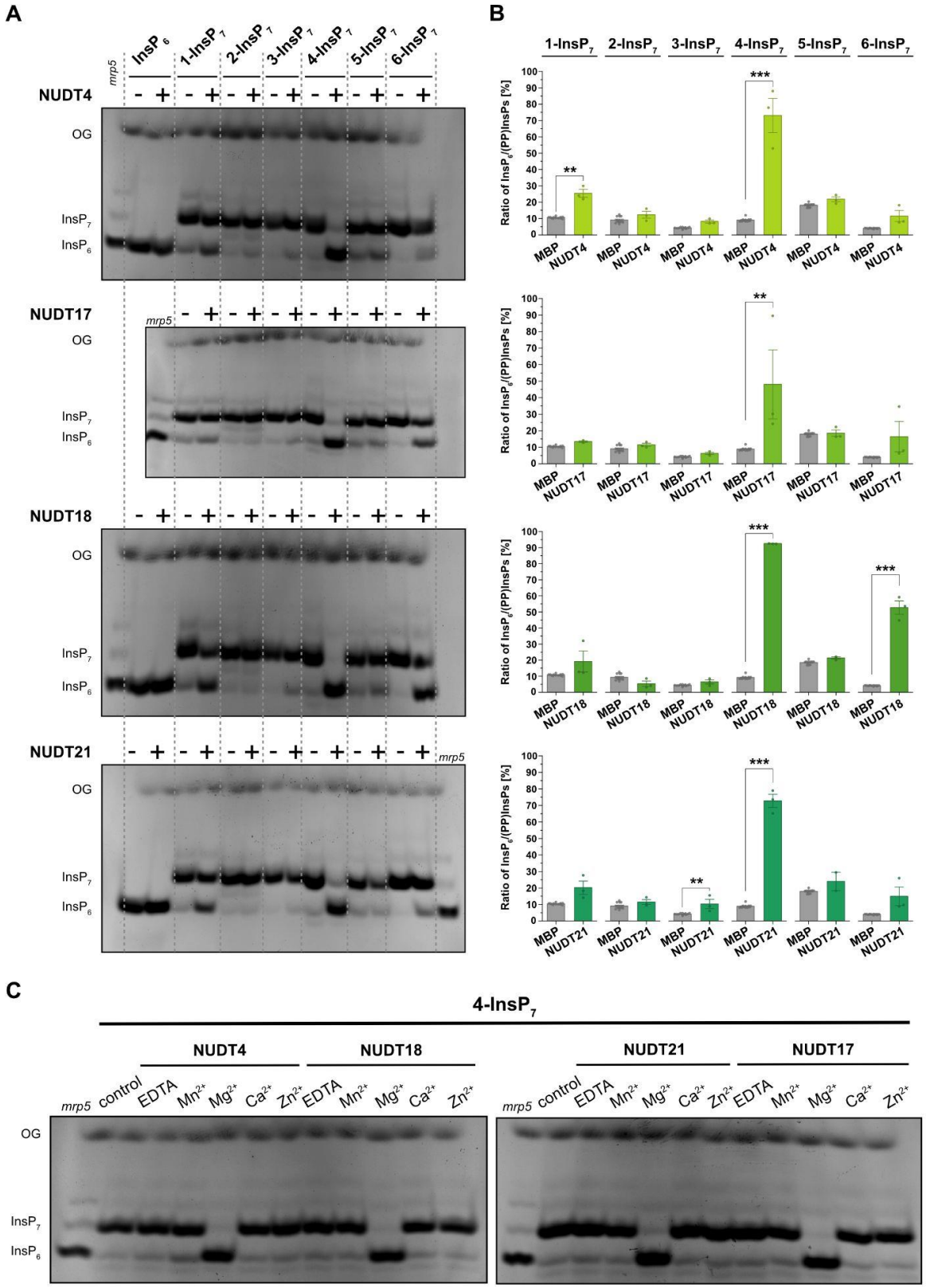

Figure 2: Subclade I NUDTs display Mg^{2+}-dependent PP-InsP phosphatase activity with high specificity for 4-$InsP_7$ *in vitro.* Recombinant His_6-MBP-tagged NUDT4, NUDT17, NUDT18 or NUDT21 was incubated with 0.33 mM $InsP_7$ and (A and B) 1 mM $MgCl_2$ or (C) either 1mM EDTA, $MnCl_2$, $MgCl_2$, $CaCl_2$, or $ZnCl_2$ at 28 °C (indicated with the plus symbol). His_8-MBP served as a negative control (indicated with the minus symbol). After 1 h, the reaction products were (A and C) separated by 33 % PAGE, and visualized by toluidine blue. A TiO_2-purified

Arabidopsis *mrp5* seed extract was used as a marker for $InsP_6$, $InsP_7$ and $InsP_8$. (B) For CE-ESI-MS analyses, samples were spiked with an isotopic standards mixture ([$^{13}C_6$] 1,5-$InsP_8$, [$^{13}C_6$] 5-$InsP_7$, [$^{13}C_6$] 1-$InsP_7$, [$^{13}C_6$] $InsP_6$, [$^{13}C_6$] 2-OH $InsP_5$). Data are presented as relative ratios of $InsP_6$ to all measured InsP/PP-InsPs and represent mean ± SEM (n ≥ 11 for MBP and n = 3 for NUDT samples, with the exception of sample NUDT21 + 5-$InsP_7$, where only 2 samples were available due to CE-ESI-MS measurement issues). Representative extracted-ion electropherograms are shown in Figure S3. Asterisks indicate values that are significantly different determined by a Dunnett's test against MBP with Šidák correction k = 4 ($P \leq 0.05$ (*); $P \leq 0.01$ (**); $P \leq 0.001$ (***)). OG: orange G.

In contrast to subclade I NUDTs, the four hydrolases of subclade II (NUDT12, NUDT13, NUDT16.1 and NUDT16.2) displayed a strong preference for 3-$InsP_7$, with the reaction product showing the same mobility as $InsP_6$ by PAGE analysis (Figure 3A), which was confirmed by CE-ESI-MS analysis (Figure 3B). However, the *in vitro* activity of NUDT16.2 was comparatively low (Figure S4), requiring a 26-fold higher protein concentration than NUDT16.1 to achieve a similar activity level. Activities against other PP-InsPs were minor or not observed, as confirmed by CE-ESI-MS analyses. Specifically, NUDT12 showed minor pyrophosphatase activity against all PP-InsPs except 5-$InsP_7$. NUDT13 and NUDT16.1 showed minor pyrophosphatase activity against 1-$InsP_7$, 4-$InsP_7$ and 6-$InsP_7$, while NUDT16.2 showed minor activities against 1-$InsP_7$ and 6-$InsP_7$ (Figure 3A and B). Similarly, to subclade I NUDTs, all subclade II NUDTs required Mg^{2+} as a cofactor to hydrolyze 3-$InsP_7$ to $InsP_6$, and no *in vitro* activity was observed in presence of other divalent cofactors, such as Ca^{2+}, Zn^{2+} and Mn^{2+} or in absence of any divalent cation (EDTA) (Figure 3C).

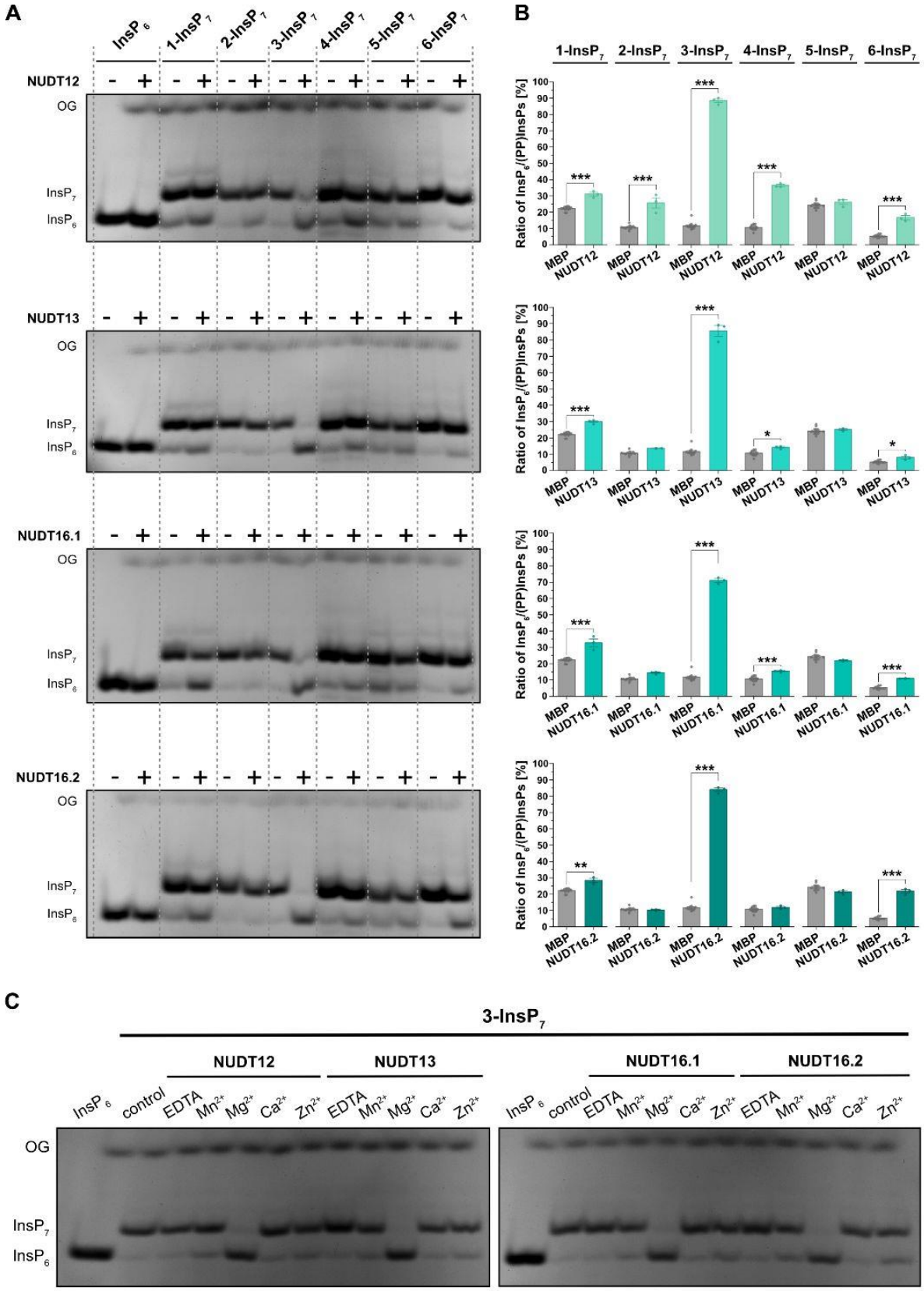

Figure 3: Subclade II NUDTs display Mg^{2+}-dependent PP-InsP phosphatase activity with high specificity for 3-$InsP_7$ *in vitro.* Recombinant His_6-MBP-tagged NUDT12, NUDT13, NUDT16.1 or NUDT16.2 was incubated with 0.33 mM $InsP_7$ and (A and B) 1 mM $MgCl_2$ or (C) either 1mM EDTA, $MnCl_2$, $MgCl_2$, $CaCl_2$, or $ZnCl_2$ at 28 °C (indicated with the plus symbol). His_8-MBP

served as a negative control (indicated with the minus symbol). After 1 h, the reaction products were (A and C) separated by 33 % PAGE and visualized by toluidine blue or (B) spiked with isotopic standards mixture ([$^{13}C_6$] 1,5-$InsP_8$, [$^{13}C_6$] 5-$InsP_7$, [$^{13}C_6$] 1-$InsP_7$, [$^{13}C_6$] $InsP_6$, [$^{13}C_6$] 2-OH $InsP_5$) for CE-ESI-MS analyses. Data represent mean ± SEM (n = 12 for MBP and n = 3 for NUDT samples). Representative extracted-ion electropherograms are shown in Figure S5. Asterisks indicate values that are significantly different determined by a Dunnett's test against MBP with Šidák correction k = 4 ($P \leq 0.05$ (*); $P \leq 0.01$ (**); $P \leq 0.001$ (***)). OG: orange G. Note that NUDT16.2 had a 16-times higher concentration (16 µM) than NUDT16.1 (0.6 µM).

Subclade II NUDT hydrolases display β-phosphate specificity also with 1,5-$InsP_8$ and 3,5-$InsP_8$, *in vitro*.

We then tested whether subclade I and II NUDTs can also hydrolyze the enantiomers of $InsP_8$ 1,5-$InsP_8$ and 3,5-$InsP_8$ in the presence of Mg^{2+}. Subclade I NUDTs, which specifically hydrolyze the 4-β-phosphate of $InsP_7$, showed only weak or no hydrolysis of both $InsP_8$ isomers *in vitro* (Figure 4A and B). Only NUDT4 and NUDT21 displayed minor hydrolytic activities against 1,5-$InsP_8$ (Figure 4A) or, in the case of NUDT4, against 3,5-$InsP_8$ (Figure 4B). In contrast, subclade II hydrolases NUDT12, NUDT13 and NUDT16 displayed robust hydrolytic activities against the 3-β-phosphate of 3,5-$InsP_8$ (Figure 4D). This activity was enantiomer-specific for NUDT12 and NUDT13, while (the two splice forms of) NUDT16 also hydrolyzed 1,5-$InsP_8$ to 5-$InsP_7$ to some extent (Figure 4C).

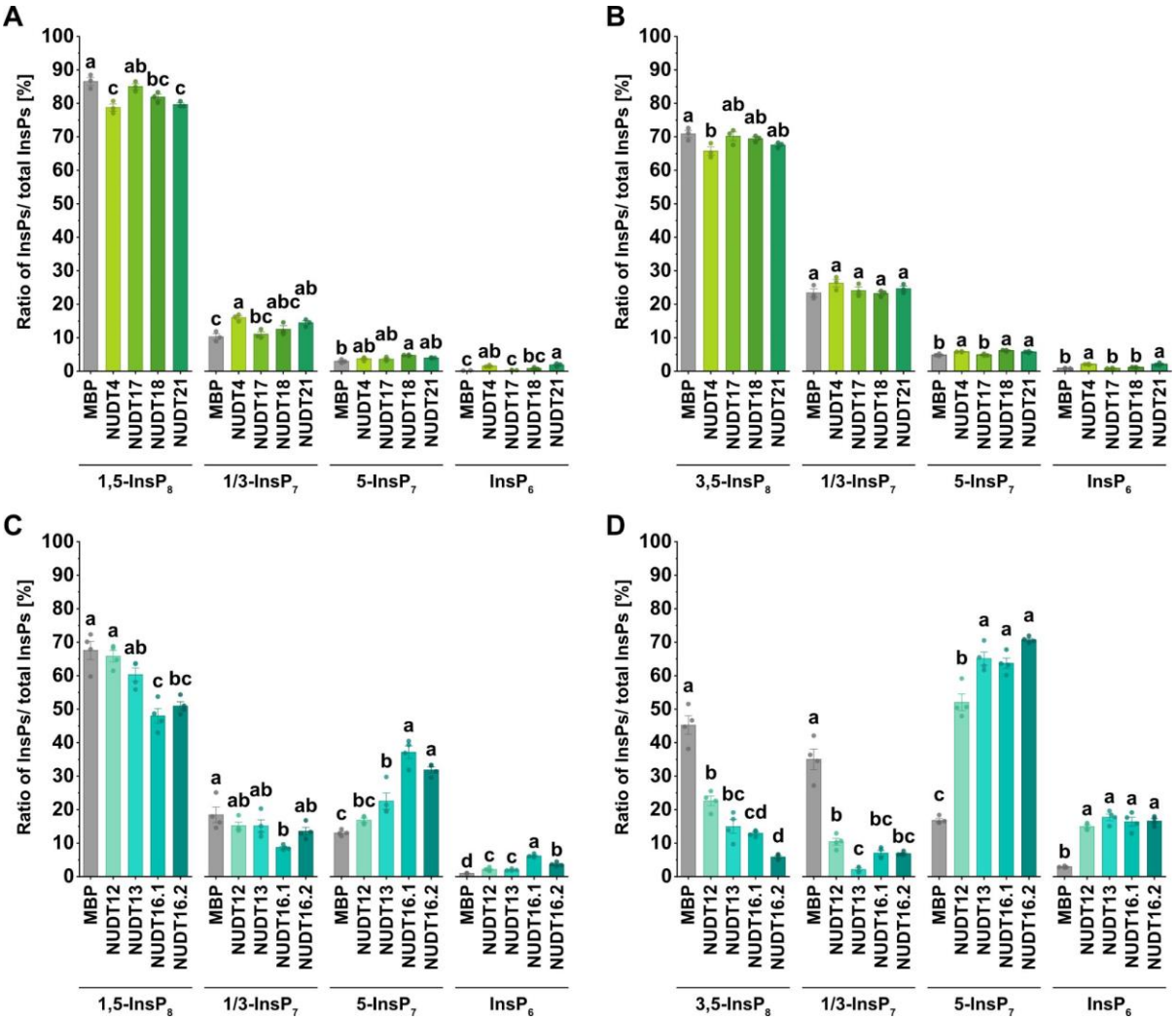

Figure 4: Arabidopsis NUDT hydrolases display differential hydrolytic activities against 1,5-$InsP_8$ and 3,5-$InsP_8$ *in vitro*. Recombinant His_6-MBP-tagged (A and B) NUDT4, NUDT17, NUDT18, NUDT21, (C and D) NUDT12, NUDT13, NUDT16.1 or NUDT16.2 protein was incubated with 0.33 mM (A and C) 1,5-$InsP_8$ or (B and D) 3,5-$InsP_8$ and 1 mM $MgCl_2$ at 28 °C. His_8-MBP served as a negative control. After 1 h, the reaction products were spiked with isotopic standards mixture ([$^{13}C_6$] 1,5-$InsP_8$, [$^{13}C_6$] 5-$InsP_7$, [$^{13}C_6$] 1-$InsP_7$, [$^{13}C_6$] $InsP_6$, [$^{13}C_6$] 2-OH $InsP_5$) and subjected to CE-ESI-MS analyses. Data represent mean ± SEM with (A and B) n = 3 and (C and D) n = 4. Representative extracted-ion electropherograms are shown in Figure S6 and Figure S7. Different letters indicate values that are significantly different determined with one-way ANOVA followed by Dunn-Šidák test with a significance level of 0.05. The peak area of 1/2/3-$InsP_7$ and of 4/5/6-$InsP_7$ was not further resolved but, since 1,5-$InsP_8$ and 3,5-$InsP_8$ isomers were used in that reaction, we conclude that the 1/2/3-$InsP_7$ peak area represents 1/3-$InsP_7$ and the 4/5/6-$InsP_7$ peak area represents 5-$InsP_7$, respectively.

At high protein concentrations, NUDT hydrolases lose some of their substrate specificity

We next investigated whether increasing protein concentration and doubling the incubation time during our *in vitro* assays would result in a loss of substrate specificity. When carrying out the reactions at these altered conditions, substrate specificities remained largely as described above (Figure S4 and Figure S8). However, we observed additional hydrolytic activities. For instance, all subclade I NUDTs showed partial pyrophosphatase activities against 5-$InsP_7$, as well as 1,5- and 3,5-$InsP_8$ (Figure S8).

Likewise, subclade II NUDT12, NUDT13 and NUDT16.1 did not only display robust activities against 3-$InsP_7$ and minor activities against $InsP_7$ isomers carrying the PP-bond at positions 1, 2, 4 and 6, respectively, but also displayed a minor 5-$InsP_7$ pyrophosphatase activity (Figure S4). In these assays, we also included the more distantly related NUDT7, previously shown to harbor ADP-ribose/NADH phosphohydrolase activity (Ogawa *et al.*, 2005). Even at a high protein concentration (~7 µM), no PP-InsP hydrolytic activity was observed for NUDT7 (Figure S4).

Higher order mutants of subclade II NUDTs display an increase in 1/3-$InsP_7$ and 5-$InsP_7$

To investigate the physiological role of subclade I and II NUDT hydrolases *in planta*, we established single and higher order loss-of-function mutants in *Arabidopsis thaliana.* The single T-DNA insertion lines *nudt17-1* and *nudt18-1*, as well as two independent T-DNA insertion lines of *nudt4* (*nudt4-1* and *nudt4-2*) and *nudt21* (*nudt21-1* and *nudt21-2*) showed no significant difference in the PP-InsP levels in comparison to the WT when grown hydroponically under optimal P conditions (Figure S9). We also generated a double mutant *nudt21-1 nudt4-1*, but also in this case we did not observe a significant effect on PP-InsP levels (Figure S9).

In order to overcome a possible functional redundancy of NUDT hydrolases, we generated higher order mutants by targeting *NUDT4*, *NUDT17*, *NUDT18* and *NUDT21*, or *NUDT12*, *NUDT13* and *NUDT16* at two different positions via CRISPR/Cas9. Each guideRNA (gRNA) was designed to target the gene at the beginning of the coding region, and upstream or within the conserved 23 amino acid region typical for NUDT hydrolases (Figure S10A and Figure S11A). The resulting higher order mutants *nudt4/17/18/21* and *nudt12/13/16* harbor mutations in all four and three targeted NUDT hydrolases, respectively (Figure S10B and Figure S11B). As depicted in Figure S10C, the resulting mutations in *nudt4/17/18/21* lead to a frameshift in all targeted open reading frames, except for line 1, where a partial deletion between the two

gRNAs results in a truncated NUDT21 lacking residues 32-74. Most of the frameshifts were caused by a single base pair mutation or larger deletions (Figure S10C). The mutations in the triple mutant *nudt12/13/16* lead to a frameshift and premature stop codon in NUDT13 and NUDT16 or, in the case of NUDT12, the start codon is already mutated (Figure S11C). None of the higher order subclade I or II *nudt* lines displayed any obvious developmental phenotype under standard growth conditions (Figure 5A). We first carried out SAX-HPLC analyses of cell extracts from [^{3}H] *myo*-inositol-labeled WT and the higher order mutants, *nudt4/17/18/21* and *nudt12/13/16*, respectively. For *nudt4/17/18/21* (line 2) plants, we did not observe any significant differences in any InsP or PP-InsP species (Figure 5B). In contrast, *nudt12/13/16* plants displayed a significant increase in $InsP_7$ (Figure 5C).

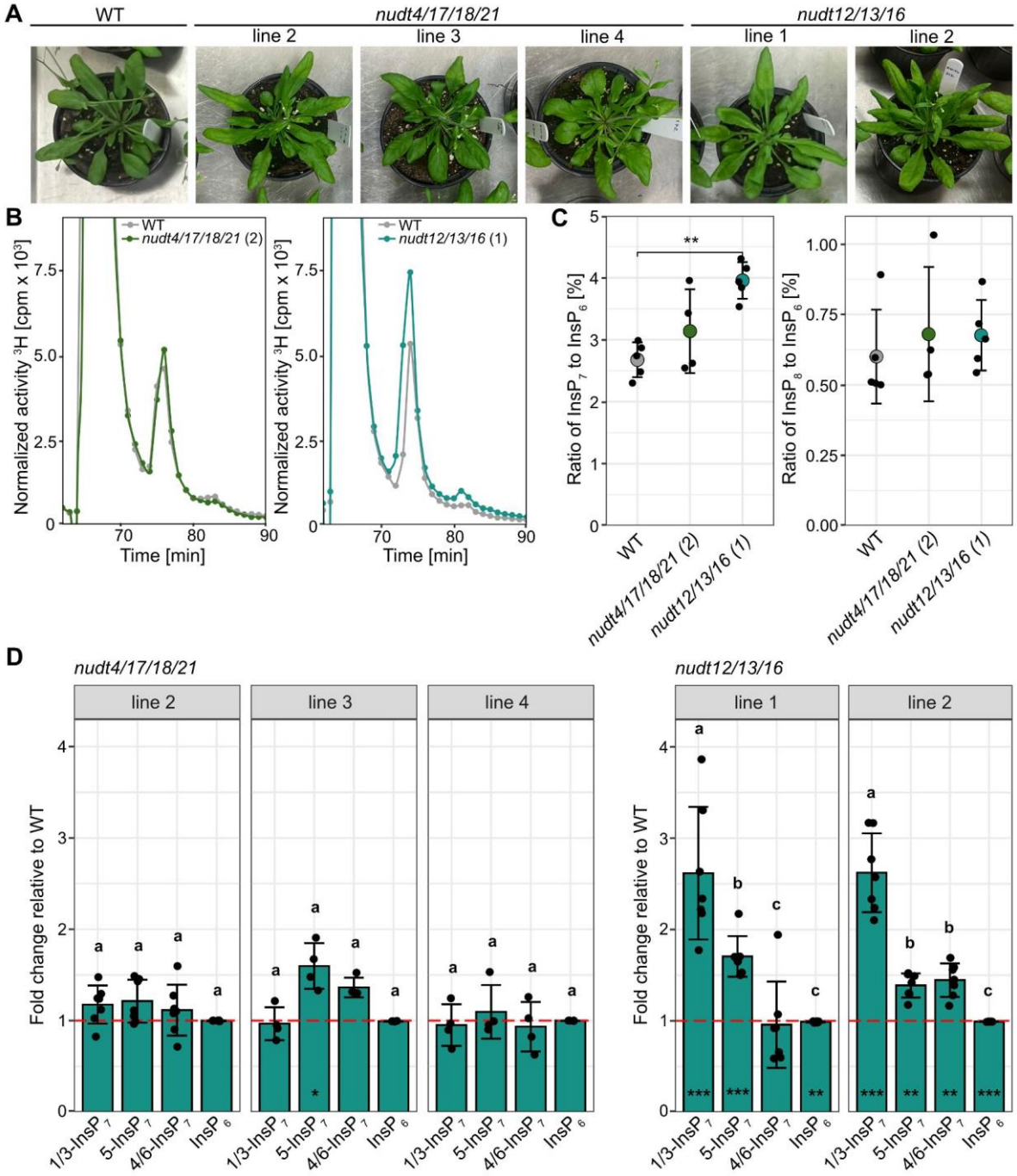

Figure 5: Higher order subclade II *nudt* mutant lines display increased 1/3-$InsP_7$ and 5-$InsP_7$ levels. (A) Photographs of 6-week-old WT and independent higher order subclade I and subclade II *nudt* mutant lines grown on peat-based substrate. (B) SAX-HPLC profiles of WT and subclade I and subclade II *nudt* mutant lines grown in liquid ½ MS medium supplemented with sucrose and [^{3}H]-*myo*-inositol. Depicted are representative SAX-HPLC runs of one line for each subclade. The experiment was repeated with similar results (n = 4 or 5). Combined data are shown in Figure 5C. (C) Relative amounts of $InsP_7$ and $InsP_8$ of WT, subclade I and subclade II NUDT mutant lines are shown as $InsP_7/InsP_6$ or $InsP_8/InsP_6$ ratios. $InsP_6$, $InsP_7$ and $InsP_8$ levels were determined by SAX-HPLC analyses and data were processed with R. Asterisks indicate significantly different $InsP_7/InsP_6$ or $InsP_8/InsP_6$ ratios compared to WT determined with Wilcoxon test for unpaired samples ($P \leq 0.01$ (**)). (D) Fold changes of various $InsP_7$ isomers and $InsP_6$ to total quantified InsPs in subclade I and subclade II NUDT mutant lines relative to WT as indicated. In this experiment, plants were grown on ½ MS agar plates

supplemented with sucrose. Asterisks indicate fold-changes to WT that are significantly different from 1 based on a Wilcoxon test for unpaired samples ($P \leq 0.05$ (*); $P \leq 0.01$ (**); $P \leq 0.001$ (***)). Compact letters display is based on a pairwise Wilcoxon test for paired samples. Fold changes of different InsPs sharing the same letter are not significantly different at $\alpha = 0.05$. The very low abundant $InsP_8$ was below or close to the detection limit in some plants and was therefore excluded from the analysis.

Because SAX-HPLC analyses cannot resolve between different $InsP_7$ isomers and rely on plants grown under sterile conditions, we employed CE-ESI-MS analyses of Nb_2O_5-purified InsPs from plants grown on a P-sufficient peat-based substrate. Under our standard growth conditions, we did not observe changes in any inositol pyrophosphate species that would be consistent in all three independent subclade I *nudt4/17/18/21* lines (Figure 5D, left panel). In contrast, subclade II *nudt12/13/16* lines showed a robust ~2.5-fold increase in 1/3-$InsP_7$ (Figure 5D, right panel), indicating that the *in vitro* hydrolytic activity against the 1/3-PP bond is of physiological relevance *in planta*. Additionally, we observed an ~1.5-fold increase in 5-$InsP_7$ and a minor but significant reduction in $InsP_6$ (Figure 5D, right panel).

Transient expression of subclade I NUDT hydrolases in *Nicotiana benthamiana* reveals PP-InsP pyrophosphatase activity and regulation of phosphate starvation responses *in vivo*

Since the *nudt4/17/18/21* lines did not show significant differences in inositol pyrophosphates, possibly due to redundancy with other enzymatic activities, we investigated the potential PP-InsP pyrophosphatase activity of NUDTs by heterologous transient expression in *N. benthamiana* leaves. To this end, we generated constructs encoding translational fusions of NUDTs from both subclades with a C-terminal 4xMyc epitope tag, driven by the strong viral CaMV 35S promoter. In agreement with our *in vitro* data (Figure 2), ectopic expression of *NUDT17*, *-18*, and *-21* significantly reduced 4/6-$InsP_7$ in *N. benthamiana* leaves, as revealed by CE-ESI-MS analyses (Figure 6A). In addition, expression of all subclade I *NUDTs* also resulted in reduced 5-$InsP_7$ levels, which is consistent with our findings that *in vitro*, all subclade I NUDTs also act as 5-$InsP_7$ pyrophosphatases at increased protein concentration (Figure 6B and Figure S8). Similarly, expression of subclade II *NUDTs*, with the exception of *NUDT13*, led to reduced levels of 4/6-$InsP_7$ and 5-$InsP_7$ in *N. benthamiana* (Figure 6A and B). Unfortunately, we were not able to quantify the very low abundant $InsP_8$ and 1/3-$InsP_7$ species in this transient expression system as these were close to or below the detection limit of our CE-ESI-MS measurements.

Experimental data extracted from the ePlant browser platform (Kilian *et al.*, 2007) indicate that *NUDT21* and *NUDT17* are induced by wounding, suggesting local regulation. Because of the role of 5-InsP$_7$ in PSR, we investigated whether transient expression of subclade I and II NUDTs could also induce local PSR. To this end, we co-expressed a *RUBY* reporter (He *et al.*, 2020) under transcriptional control of a *Solanum lycopersicum SPX2* promoter fragment with NUDT hydrolases in *N. benthamiana* leaves (Figure 6C). Heterologous expression of Arabidopsis *PFA-DSP1*, which encodes a *bona fide* 5PP-InsP pyrophosphatase hydrolysing the 5-β-phosphate of 5-InsP$_7$, as well as 1,5-InsP$_8$ and 3,5-InsP$_8$ (Gaugler *et al.*, 2022), served as a positive control (Figure 6D).

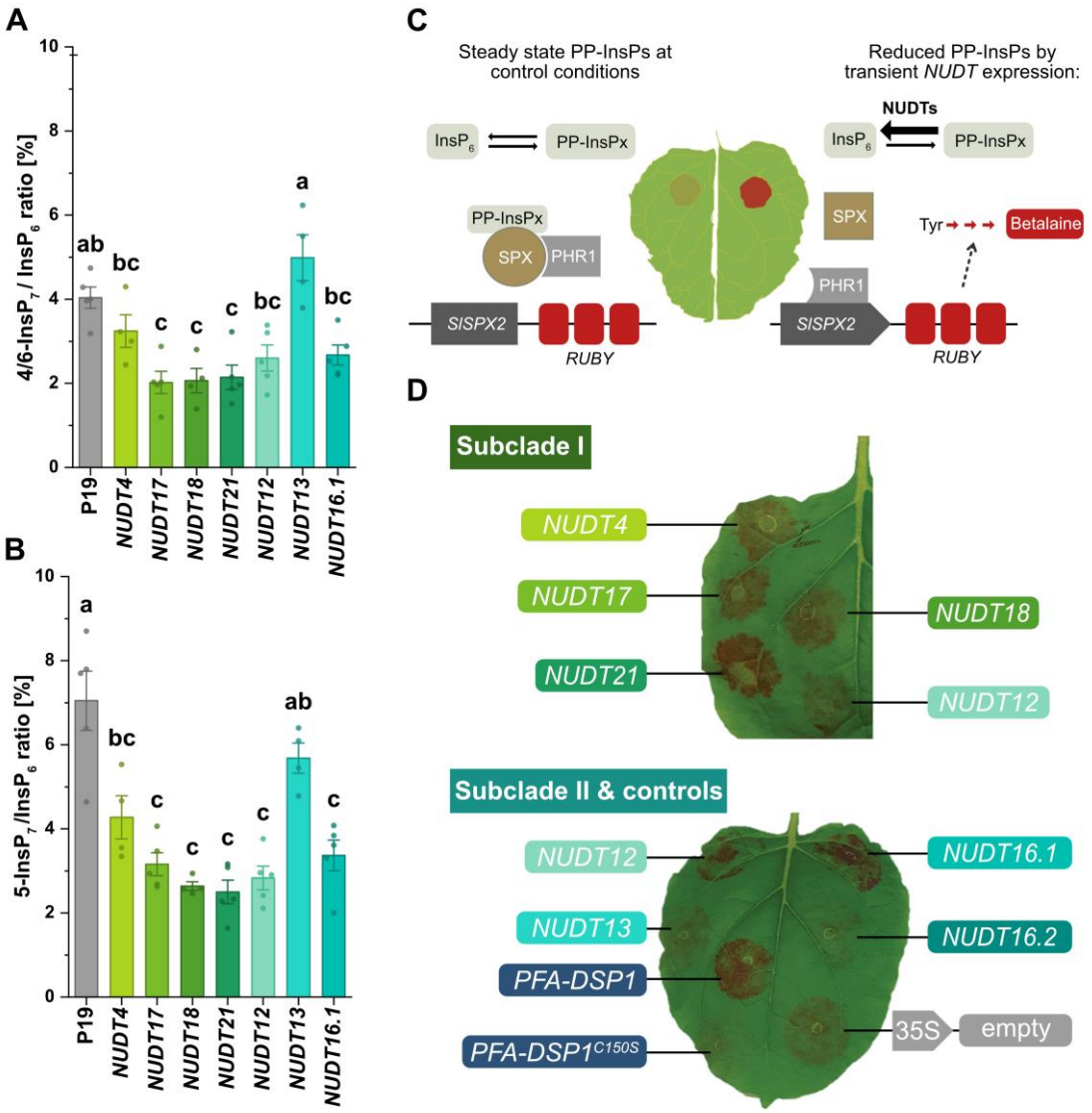

Figure 6: Transient expression of NUDTs in *N. benthamiana* reveals PP-InsP activity and regulation of phosphate starvation responses. (A and B) Heterologous expression of subclade I and II NUDTs results in 4/6-PP-InsP$_7$ and 5-PP-InsP$_7$ turnover *in planta* and induces local PSR. The silencing inhibitor P19 alone or together with NUDTs were transiently expressed in *N. benthamiana* leaves. 2-3 days post infiltration (dpi) (PP-)InsPs were purified with Nb_2O_5 beads, spiked with isotopic standards mixture ([$^{13}C_6$] 1,5-InsP$_8$, [$^{13}C_6$] 5-InsP$_7$, [$^{18}O_2$] 4-InsP$_7$,

[$^{13}C_6$] 1-InsP$_7$, [$^{13}C_6$] InsP$_6$, [$^{13}C_6$] 2-OH InsP$_5$) and subjected to CE-ESI-MS analyses. Data represent mean ± SEM (n ≥ 4). Different letters indicate values that are significantly different determined with one-way ANOVA followed by Dunn-Šidák test with a significance level of 0.05. Representative extracted-ion electropherograms are shown in Figure S12. (C) Schematic representation of PSR reporter assay in *N. benthamiana* leaves, in which a reduced PP-InsP concentration enables PHR1 to bind a P1BS binding site in the *SlSPX2* promoter (Solyc12g009480; LOC101257836) driving the expression (dotted arrow) of a *RUBY* reporter cassette (encoding three different proteins CYP76AD1, DODA and a glycosyltransferase) that catalyze the stepwise synthesis (red arrows) of a red betalain pigment. (D) Transient co-expression of the *RUBY* reporter with subclade I or subclade II *NUDT* hydrolase genes under the transcriptional control of the viral CaMV 35S promoter. Co-expression with *PFA-DSP1* served as a positive control while co-expression with *PFA-DSP1*^{C150S} encoding the catalytic inactive protein or an empty vector served as negative controls. The picture was taken 2 dpi (upper leaf) or 3 dpi (bottom leaf). Note that subclade I *NUDT12* was expressed in both leaves for comparison. Three independent replicates are shown in Figure S13.

The induction of this PSR response was dependent on the catalytic activity of PFA-DSP1 since the construct encoding the catalytically inactive variant, PFA-DSP1^{C150S} (Gaugler *et al.*, 2022), failed to induce PSR (Figure 6D). Notably, heterologous expression of all subclade I *NUDTs* caused robust red staining reporting local activation of PSR (Figure 6D). Likewise, expression of *NUDT12* and the active splice variant 1 of *NUDT16* also resulted in red staining, albeit generally at lower intensity (Figure 6D). In contrast, expression of *NUDT13* or the less active splice variant 2 of *NUDT16* failed to activate PSR as compared to the empty vector or PFA-DSP1^{C150S} negative controls (Figure 6D).

Subclade II NUDTs are involved in P- and Fe-homeostasis

We then investigated the consequences of increased 1/3-InsP$_7$ and 5-InsP$_7$ in *nudt12/13/16* lines. Under standard growth conditions, none of the higher order subclade I or II *nudt* lines displayed any obvious developmental phenotype (Figure 5A). Since 5-InsP$_7$ has been shown to bind and activate SPX domains (Wild *et al.*, 2016) and is suggested to partially compensate for the loss of InsP$_8$ in suppressing PSR in Arabidopsis (Riemer *et al.*, 2021), we performed a mineral element analysis of WT and two independent *nudt12/13/16* lines grown under P-sufficient conditions on a peat-based substrate. In agreement with a role of 5-InsP$_7$ in suppressing PSR, we indeed observed decreased shoot P accumulation in both lines, as determined by ICP-OES analysis (Figure 7A). No consistent changes (i.e., changes in both independent lines) were observed for other macronutrients (Figure 7A). However, among the micronutrients, shoot iron (Fe) concentration was decreased by 53 % in *nudt12/13/16* plants (Figure 7B). To raise further evidence for the role of subclade II NUDTs in PSR regulation, we checked whether they are transcriptionally responsive to the plant's P status. For this purpose, we grew plants in hydroponic culture and subjected them to sufficient or deficient P$_i$ conditions,

or deficient P_i followed by P_i resupply, as reported previously (Riemer *et al.*, 2021). Notably, transcripts of all subclade II NUDTs increased under P_i-deficient conditions in shoots (Figure 7C). Additionally, elevated levels of *NUDT13* and *NUDT16* transcripts were also observed in roots of Arabidopsis WT plants grown under P_i-deficient conditions (Figure 7C). When P_i-deficient plants were resupplied with P_i for 12 hours, the expression levels of all *NUDTs* were comparable or even below the levels observed in plants grown under sufficient P_i (Figure 7C).

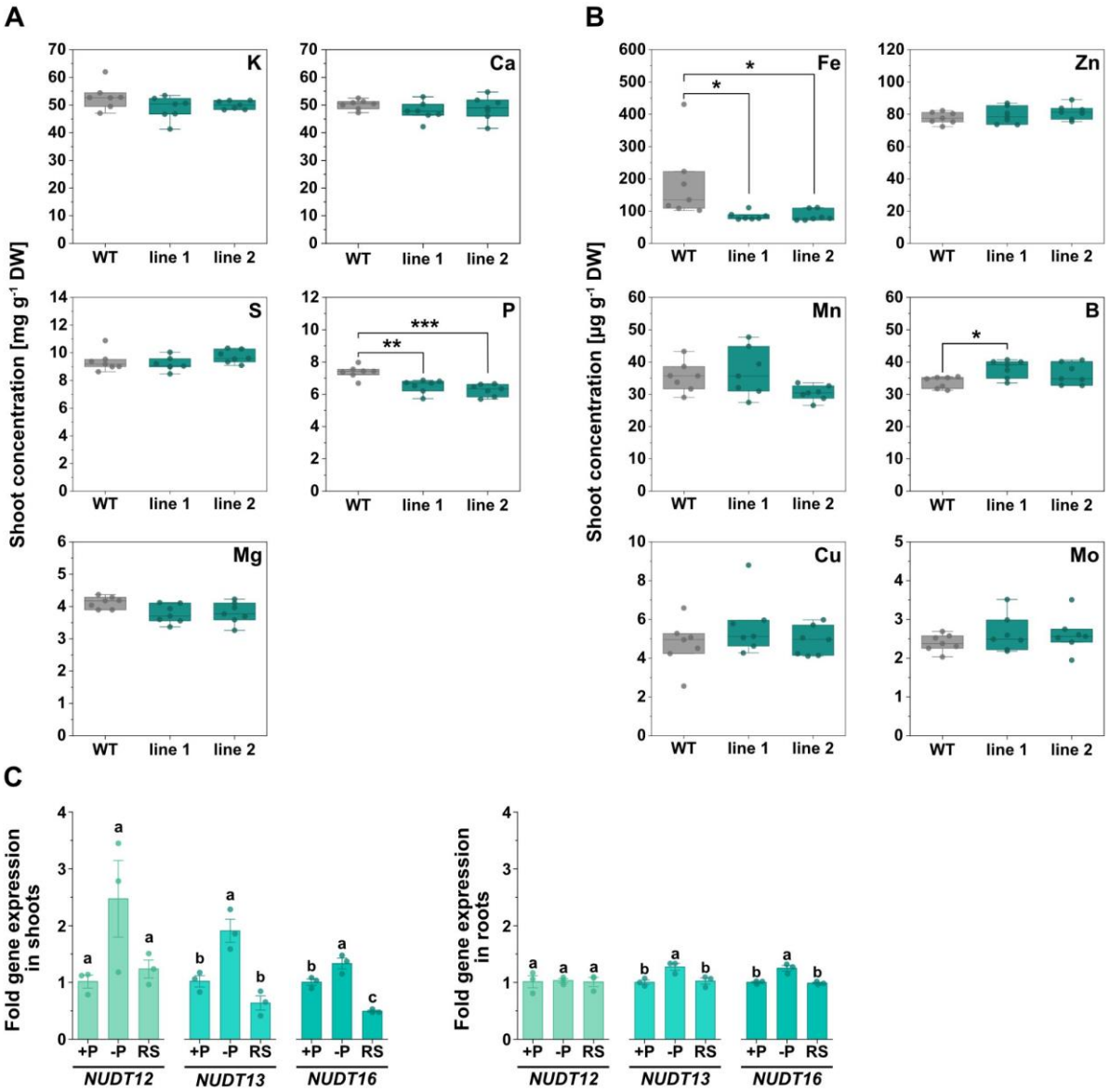

Figure 7: Subclade II NUDTs are involved in P and Fe homeostasis and are upregulated by P-deficiency. (A) Shoot concentration of the indicated mineral macronutrients. (B) Shoot concentration of the indicated micronutrients. Each line is represented by seven biological replicates (n = 7). Asterisks indicate values that are significantly different determined with one-way ANOVA followed by Dunn-Šidák test (P ≤ 0.05 (*); P ≤ 0.01 (**); P ≤ 0.001 (***)). Plants were grown for four weeks on a peat-based substrate. (C) Arabidopsis WT plants were grown under sufficient P (indicated with +P), under deficient conditions (indicated with -P) or grown under deficient conditions and resupplied with P_i for 12 hours (indicated with RS). The gene

expression of *NUDT12*, *NUDT13* and *NUDT16* are displayed by means ± SEM (n = 3). Different letters indicate values that are significantly different determined with one-way ANOVA followed by Dunn-Šidák test with a significance level of 0.05.

Transcriptome analyses suggests subclade II NUDT-dependent PP-InsPs act primarily as negative regulators of gene expression and also modulate PSR-independent functions

To gain more insights into subclade II NUDTs and, thus, potentially 1/3-InsP$_7$-related processes, we conducted RNA-seq experiments using shoots of two *nudt12/13/16* triple mutants and the corresponding WT, grown on P-sufficient peat-based substrate. We identified 258 differentially expressed genes (DEGs) common to both mutant lines, compared to WT plants (Figure 8 and Supplementary File 2). Of these, the majority represent downregulated genes (206), while 49 genes were upregulated. We observed a number of PSR-related genes, the purple acid phosphatase *PAP1*, *ATL80* and *ZAT6*, all of which were downregulated (Table S2 and S3). In addition, we observed a number of Fe-related genes to be differentially regulated (Tables S3 and S4).

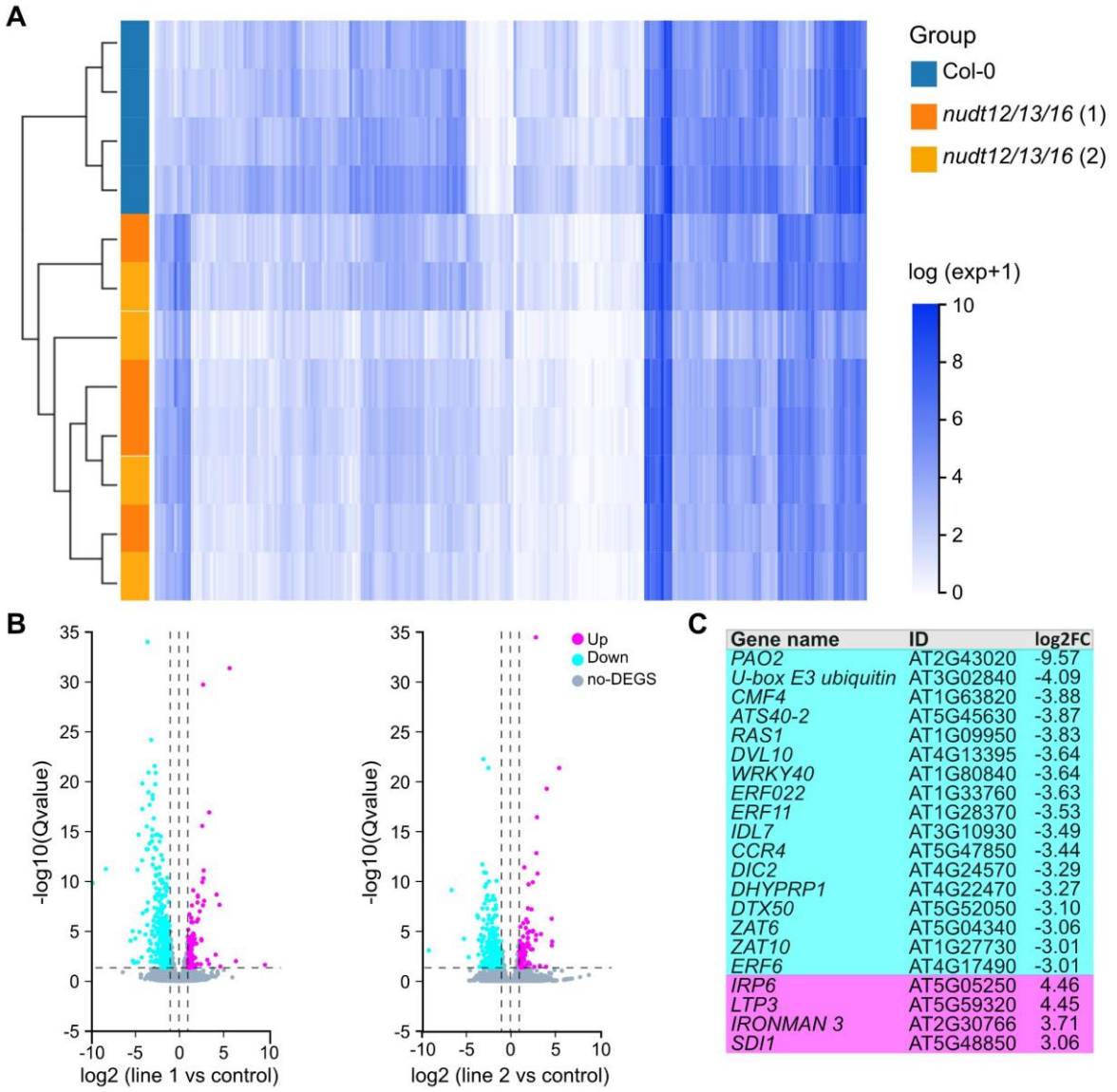

Gene name	ID	log2FC
PAO2	AT2G43020	-9.57
U-box E3 ubiquitin	AT3G02840	-4.09
CMF4	AT1G63820	-3.88
ATS40-2	AT5G45630	-3.87
RAS1	AT1G09950	-3.83
DVL10	AT4G13395	-3.64
WRKY40	AT1G80840	-3.64
ERF022	AT1G33760	-3.63
ERF11	AT1G28370	-3.53
IDL7	AT3G10930	-3.49
CCR4	AT5G47850	-3.44
DIC2	AT4G24570	-3.29
DHYPRP1	AT4G22470	-3.27
DTX50	AT5G52050	-3.10
ZAT6	AT5G04340	-3.06
ZAT10	AT1G27730	-3.01
ERF6	AT4G17490	-3.01
IRP6	AT5G05250	4.46
LTP3	AT5G59320	4.45
IRONMAN 3	AT2G30766	3.71
SDI1	AT5G48850	3.06

Figure 8: Shoot transcriptome analyses of *nudt12/13/16* triple mutants suggest subclade II NUDT-dependent PP-InsPs act primarily as negative regulators of gene expression. (A) Clustered Heatmap of differentially expressed genes (DEGs) filtered by Q<0.05 and log2 fold change (|log2FC| > 1). The horizontal axis represents the log2 (expression value + 1) for the samples based on TPM (Transcripts Per Million) expression value, while the vertical axis represents genes. In the default color scheme, dark blue indicates higher expression levels and white indicates lower expression levels. Mutant lines are represented in orange and light orange, and are clustered together, while the control is depicted in blue. Each line is represented by four biological replicates (n = 4). (B) Volcano plot comparing triple mutant line 1 and 2 to WT. The X-axis represents the log2FC values, and the Y-axis shows -log10-transformed significance values. Magenta dots indicate upregulated DEGs, cyan dots indicate downregulated DEGs, and gray dots indicate non-DEGs. (C) The table displays genes that showed strongest differential expression (|log2FC| > 3) of only downregulated and upregulated genes with known annotations. A complete list with all genes in this category of strongest differential expression is shown in Table S3. All plants used in these analyses, including wildtype controls, were grown on a peat-based substrate.

However, PSR genes only represented a minor subset of DEGs in *nudt12/13/16* triple mutants. Gene Ontology (GO) enrichment analysis revealed an overrepresentation of terms related to defense and associated processes, such as reactive oxygen species (ROS), wounding, systemic acquired resistance, and responses to chitin and insects, in both independent lines (Figure 9 and Figure S14). Additionally, transcripts encoding proteins involved in responses to hypoxia, oxidative stress, ozone, and anaerobic respiration—terms also associated with ROS—were similarly enriched (Figure 9 and Figure S14).

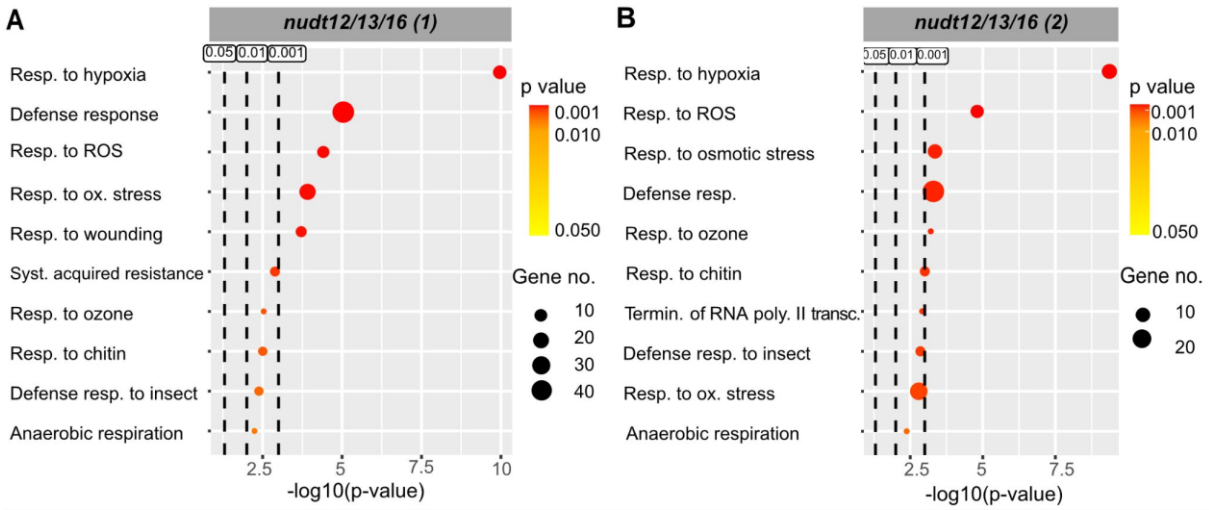

Figure 9: (A and B) Gene Ontology (GO) enrichment analysis suggests subclade II NUDT-dependent PP-InsPs regulate PSR-unrelated processes with numerous genes involved in plant defense and related GO terms. Shown is a GO enrichment analysis of DEGs with Q < 0.05 and (|log2FC| > 1), based on Biological Processes (BP) for *nudt12/13/16* triple mutant lines 1 and 2. The X-axis represents the statistical significance of these GO terms in -log10 (p-value), while the Y-axis lists the GO terms. Bubble size indicates the number of DEGs annotated to each GO term, and the graph highlights three significance thresholds: 0.05, 0.01, and 0.001. The color of the bubbles corresponds to the p-value, with red indicating more significant enrichment (Resp. = response, ROS = reactive oxygen species, ox. = oxidative, syst.= systematic, termin.=termination, poly.=polymerase).

The 3PP- position of PP-InsPs is also vulnerable to enzymatic activities unrelated to subclade II NUDTs

Because RNA-seq data of *nudt12/13/16* lines indicated misregulation of gene expression unrelated to PSR, we wondered whether increased PP-InsPs other than 5-InsP$_7$ that might be responsible for these transcriptional phenotypes represent preferred substrates of known enzymes involved in PP-InsP metabolism. Recent work by Withfield and colleagues (2024) demonstrated that both potato and Arabidopsis ITPK1 can phosphorylate 1-InsP$_7$ and 3-InsP$_7$ to 1,5 InsP$_8$ and 3,5-InsP$_8$, respectively. To address this intriguing activity of ITPK1 further, we tested all six synthetic InsP$_7$ isomers and, in agreement with these findings, observed a robust

phosphorylation of 3-$InsP_7$, presumably resulting in the generation of 3,5-$InsP_8$ (Figure 10A). Besides, we detected a minor activity with 1-$InsP_7$ and no detectable activity against any other $InsP_7$ isomer, suggesting a highly specific 3-$InsP_7$ kinase activity of ITPK1 (Figure 10A). Likewise, human ITPK1, for which we had previously identified $InsP_6$ kinase activity (Laha *et al.*, 2019), also phosphorylated 3-$InsP_7$, suggesting a high degree of evolutionary conservation of this activity (Figure 10B). We also investigated whether ITPK1 catalyzes a 3,5-$InsP_8$/ADP phosphotransferase activity leading to the production of ATP and 3-$InsP_7$, as reported earlier by Withfield and colleagues (2024). Notably, we observed a robust generation of $InsP_7$ (presumably 3-$InsP_7$) when incubating 3,5-$InsP_8$ and ADP in presence of human ITPK1. While we did not observe significant 3,5-$InsP_8$/ADP phosphotransferase activity of Arabidopsis ITPK1 under our experimental conditions, we detected phosphotransferase activity of the recombinant Arabidopsis VIH2 kinase domain, presumably resulting in the generation of ATP and 5-$InsP_7$ (Figure 10B). In summary, our findings and those by Withfield and colleagues (2024) suggest that 3PP-InsP species represent preferred products and substrates of various plant enzymes and that some of their activities appear to be evolutionarily conserved.

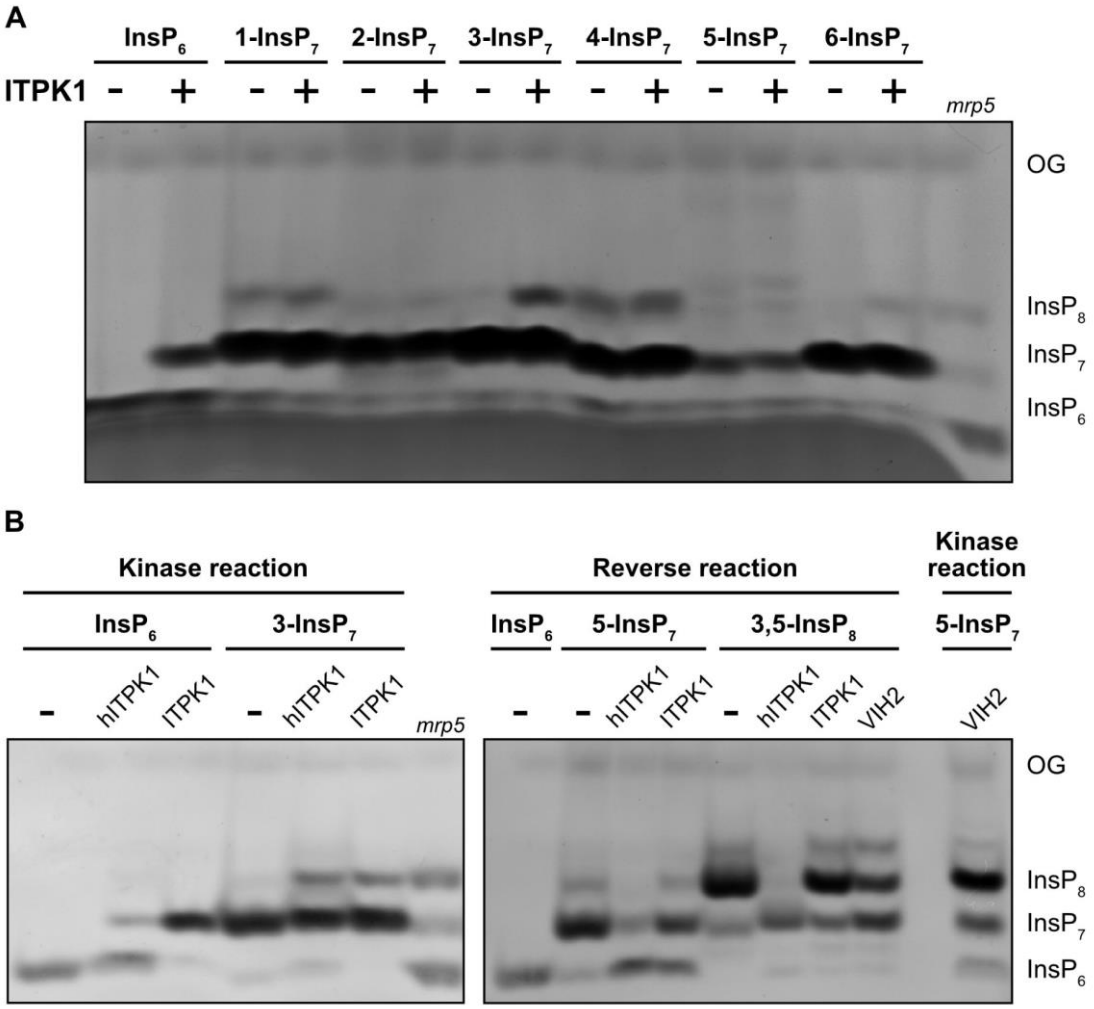

Figure 10: 3PP-InsP species are preferred substrates for evolutionary conserved kinase and ADP phosphotransfer reactions. (A) Kinase assay with recombinant His_8-MBP-ITPK1 and $InsP_6$ or $InsP_7$ species as indicated. (B) Kinase assay (kinase reaction) and PP-InsP/ADP phosphotransfer assay (reverse reaction) with recombinant His_8-MBP-ITPK1, His_8-MBP-VIH2 and His_8-MBP-hsITPK1 and 1 mM of the indicated (PP)-InsP species. (A, B) After 6 h at 25°C, the reaction products were separated by 33 % PAGE, and visualized by toluidine blue staining. His_8-MBP served as a negative control (indicated with the minus symbol). KD: kinase domain, OG: orange G.

NUDT effectors of pathogenic ascomycete fungi display a substrate specificity reminiscent of subclade I NUDTs

Because the RNA-seq data of *nudt12/13/16* lines revealed a large portion of DEGs involved in plant defense (Figure 9A and B), we wondered whether plant pathogens might be able to directly interfere in PP-InsP homeostasis. Notably, recent work by McCombe and colleagues showed that NUDT hydrolase-type effectors of plant pathogenic fungi contribute to fungal virulence (McCombe *et al.*, 2023). The authors proposed that a 5-$InsP_7$ pyrophosphatase activity and the local induction of PSR at the infection site might be responsible for this phenotype (McCombe *et al.*, 2023). To further investigate the substrate specificity of fungal NUDT effectors, we generated His_6-tagged recombinant proteins for NUDTs from *Magnaporthe oryzae* (the causal agent of rice blast), *Colletotrichum graminicola* (which causes anthracnose leaf blight in maize and wheat), *Colletotrichum higginsianum* (a fungus that infects many species of the Brassicaceae, including *Arabidopsis thaliana*) and *Colletotrichum tofieldiae* (a root endophyte infecting *Arabidopsis thaliana*). In line with their potential role in inducing phosphate starvation responses, we observed robust activity against 5-$InsP_7$ under our *in vitro* conditions, corroborating the findings of McCombe and colleagues (2023). Furthermore, we noted substrate specificities reminiscent of subclade I NUDTs: while 2-$InsP_7$ and 3-$InsP_7$ were largely resistant to these NUDT effectors, all four enzymes displayed robust 4-$InsP_7$ and 6-$InsP_7$ pyrophosphatase activities, alongside partial pyrophosphatase activity against 1-$InsP_7$ (Figure 11A-D).

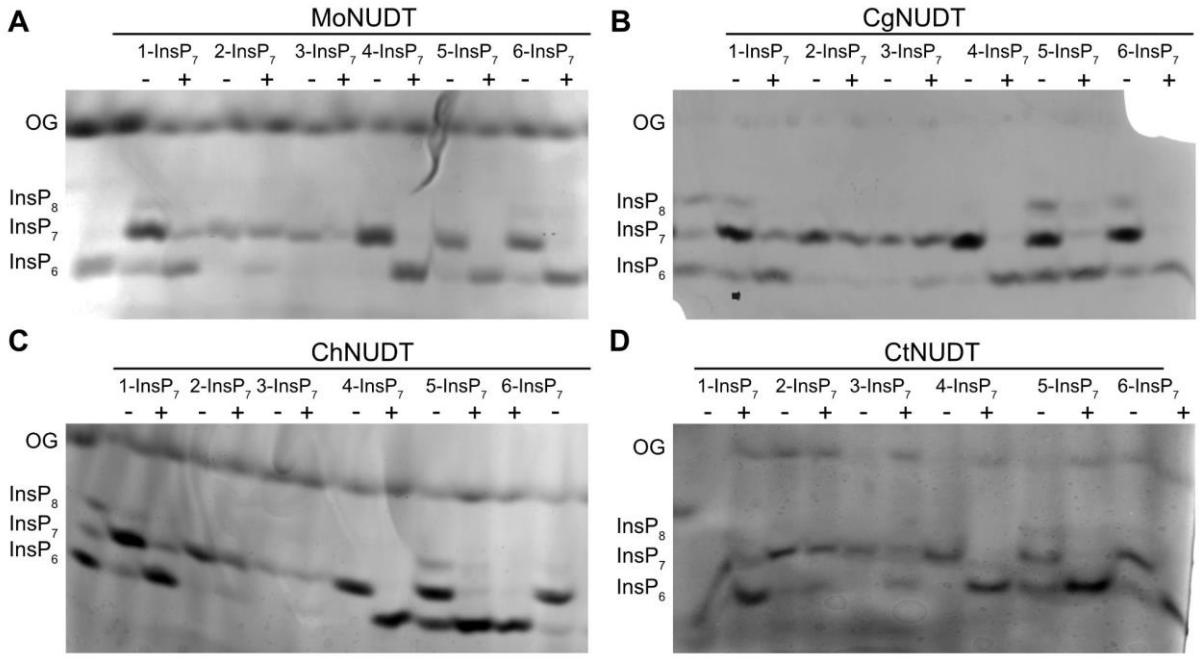

Figure 11: Fungal NUDT effectors show similar substrate specificities as NUDTs of clade I. Recombinant His_6-tagged MoNUDT (A), CgNUDT (B), ChNUDT(C) or CtNUDT (D) was incubated with 0.25 mM $InsP_7$. The minus symbol shows control reactions where no protein was added. After 45 min, the reaction products were separated by 33 % PAGE, and visualized by toluidine blue staining. A TiO_2-purified Arabidopsis *mrp5* seed extract was used as a marker for $InsP_6$, $InsP_7$ and $InsP_8$. OG: orange G.

Discussion

PP-InsPs were detected for the first time in mammalian cells more than 30 years ago by treating pancreatic rat tumor AR4-2J cells with high doses of sodium fluoride (NaF), (Menniti *et al.*, 1993). The authors used NaF, supposedly inhibiting mammalian PP-InsP pyrophosphatases, to show a massive turnover of these messengers, suggesting that, in mammalian cells, about 50% of the $InsP_6$ pool (comprising about 50-100 µM) is converted to a low abundant pool of PP-InsPs (0.1 - 2 µM) within one hour. In yeast, recent ^{18}O-water labeling experiments demonstrated rapid incorporation of label into 1,5-$InsP_8$ and 5-$InsP_7$ reaching equilibrium within 15-20 min, suggesting a high turnover of these messengers (Kim *et al.*, 2024), as in mammalian cells. In plants, despite important functions of PP-InsPs in defense, auxin-perception and regulation of PSR, little is known about the turnover of these metabolites. While PFA-DSP-type hydrolases have been shown to execute *in vitro* pyrophosphatase activity with a high specificity against the 5PP-moiety of PP-InsPs (Wang *et al.*, 2022; Gaugler *et al.*, 2022), a physiological role in 5-$InsP_7$ or 1,5-$InsP_8$ turnover *in planta* still remains unresolved. Hydrolases involved in the turnover of 4-$InsP_7$, 6-$InsP_7$ or 3-$InsP_7$ have not yet been presented until now. Using an affinity pull-down assay with stable 5PCP-

$InsP_5$ beads, we isolated previously proposed PP-InsP-interacting proteins, including AtVIH1/AtVIH2 (Laha *et al.*, 2015; Zhu *et al.*, 2019), AtSPX2 (Ried *et al.*, 2021), and AtCOI1 (Laha *et al.*, 2015, 2016) from Arabidopsis extracts. We also isolated AtIPK2alpha and AtIPK2beta, which have been shown to be involved in the synthesis of lower InsP species and so far not been linked to PP-InsP binding or synthesis *in planta* (Stevenson-Paulik *et al.*, 2002, 2005). However, recent findings show that Arabidopsis IPK2alpha synthesizes 4/6-$InsP_7$ from $InsP_6$ *in vitro* and may regulate 4/6-$InsP_7$ *in vivo* (Yadav *et al.*, 2023). In addition to those targets, the assay also revealed five *Arabidopsis thaliana* NUDT hydrolases with previously unknown functions as novel interaction partners of 5PCP-$InsP_5$: NUDT4, -16, -17, -18, and -21 (Table S1).

The NUDT hydrolase family is a conserved group of proteins found across eukaryotes, bacteria, archaea and viruses that target diphospho-bonds of different nucleoside derivatives, like nucleotide sugars (Bessman *et al.*, 1996; Muñoz *et al.*, 2006; Ogawa *et al.*, 2008), dinucleotide polyphosphates (Bessman *et al.*, 1996; Yoshimura *et al.*, 2007), nucleotide coenzymes (Bessman *et al.*, 1996; Ogawa *et al.*, 2005; Ishikawa *et al.*, 2009) and nucleoside triphosphates (Bessman *et al.*, 1996). In addition, NUDTs also target non-nucleoside pyrophosphate substrates, such as 5-phosphoribosyl 1-pyrophosphate (Fisher *et al.*, 2002), dihydroneopterin triphosphate (Klaus *et al.*, 2005) and diphosphoinositol polyphosphates (Safrany *et al.*, 1998, 1999). In Arabidopsis, 29 genes were identified encoding NUDT proteins, whereas one member, NUDT26 (At2g04440), harbors only partly the conserved NUDT motif (GX_5EX_7REUXEEXGU, where U represents a hydrophobic residue, such as leucine, isoleucine, or valine, and X represents any amino acid) (Bessman *et al.*, 1996; Gunawardana *et al.*, 2009; Yoshimura & Shigeoka, 2015). Some NUDT proteins in plants have been characterized and shown to hydrolyze ADP-glucose (Muñoz *et al.*, 2006), capped mRNA (7-methyl GTP) (Xu *et al.*, 2006), oxidized deoxyribonucleotide (8-oxo-dGTP) (Yoshimura *et al.*, 2007), ADP-ribose (Ge *et al.*, 2007; Ogawa *et al.*, 2009; Ishikawa *et al.*, 2009), NADH (Ge *et al.*, 2007; Ishikawa *et al.*, 2009, 2010), FAD (Maruta *et al.*, 2012), GDP-mannose (Tanaka *et al.*, 2015) and NADPH (Maruta *et al.*, 2016)(Maruta *et al.*).

We identified largely different substrate specificities of NUDTs investigated in this study, with a preference of subclade I NUDTs for 4-$InsP_7$ and a preference of subclade II for 3-$InsP_7$ (Figures 2 and 3, respectively). Considering that subclade II NUDTs only display a minor activity against 1-$InsP_7$ and that higher order mutants of this subclade show a robust 2.5-fold increase in 1/3-$InsP_7$, our findings suggest that Arabidopsis might synthesize 3-$InsP_7$ - possibly in addition to its canonical enantiomeric isomer 1-$InsP_7$ also found in yeast and mammals (Mulugu *et al.*, 2007; Fridy *et al.*, 2007; Dollins *et al.*, 2020). In favor of this idea are observations by Whitfield et al. (2024) and presented in this manuscript that 3-$InsP_7$ is also the

preferred $InsP_7$ substrate recognized by the $InsP_6$ kinases ITPK1 (Figure 10A), a specificity that appears to be conserved from plants to humans (Figure 10B). However, conclusions regarding isomer identity are indirect, and we propose that the enantiomer selectivity of these different subclade I and II NUDTs might be used as tools to address the enantiomer identities of plant 4/6-$InsP_7$ and 1/3-$InsP_7$ directly by *in vitro* digests of plant-purified PP-InsPs and the help of synthetic [$^{13}C_6$]-labeled $InsP_7$ standards spiked into these reactions. As 4/6-$InsP_7$ has recently also been identified in mammalian tissues (Qiu *et al.*, 2023) and 1/3-$InsP_7$ awaits clarification in animals as well, there might be a wider interest for such tools. Interestingly, human DIPP1 (alternative name NUDT3), the NUDT hydrolase which is most closely related to yeast Ddp1 and also subclade I and II Arabidopsis NUDTs, showed robust hydrolytic activity towards 1-$InsP_7$ and 3-$InsP_7$ *in vitro* (Dollins *et al.*, 2020).

Initially, we were surprised by a minor yet significant increase in 5-$InsP_7$ levels in the independent triple mutants of subclade II NUDTs (Figure 5D), given the poor activity of these NUDTs against 5-$InsP_7$ *in vitro* (Figure 3A and B). However, transient expression of NUDT12 or NUDT16.1 in *N. benthamiana* resulted in a decrease in 5-$InsP_7$, suggesting activity against this isomer (Figure 6B). Moreover, when using higher protein concentrations, we detected 5-$InsP_7$ pyrophosphatase activity in all subclade II NUDTs, but not in the more distantly related NUDT7 (Figure S4). Collectively, these findings suggest that NUDTs exhibit direct pyrophosphatase activity also toward 5-$InsP_7$. We hypothesize that this "side activity" has physiological significance, as the concomitant decrease in shoot P levels observed in both independent subclade II *nudt12/13/16* lines (Figure 7A) aligns with the role of 5-$InsP_7$ in suppressing PSR in yeast and plants (Wild *et al.*, 2016; Riemer *et al.*, 2021). The key question arising from these experiments is the role of 4/6-$InsP_7$ and 1/3-$InsP_7$ in plants. Since our independent subclade I *nudt4/17/18/21* lines yielded inconsistent PP-InsP results, we were unable to address the function of 4/6-$InsP_7$. However, in both independent subclade II *nudt12/13/16* lines, we observed a robust increase in 1/3-$InsP_7$, in addition to the minor increase in 5-$InsP_7$ (Figure 5D).

Our RNA-seq experiment with two independent *nudt12/13/16* triple mutants revealed that downregulated genes represented by far the larger fraction, consistent with the concept that PP-InsPs, such as 5-$InsP_7$ and $InsP_8$, act as negative regulators of gene expression (Dong *et al.*, 2019; Zhu *et al.*, 2019; Ried *et al.*, 2021; Riemer *et al.*, 2021). While we observed a number of DEGs involved in PSR (Table S2) that might explain the decreased P-content in shoots (Figure 7A), the majority of DEGs did not show any obvious connection with P_i signaling. A closer examination of the genes showing the highest degree of downregulation or upregulation (log2FC < -3 or > +3, Figure 8B and Table S3) revealed additional insights into the possible roles of elevated PP-InsP levels in these lines. Many downregulated genes were related to

ethylene signaling and senescence (e.g., *ATS40-2*, *ERF022*, *ERF11*, *ERF6*), while another set, in agreement with the GO enrichment results, was defense-related (e.g., *WRKY40*, *PAO2*, *IDL7*, *DHYPRP1*) (Table S3). Future research will need to explore the functional relevance of these transcriptional changes. Infection assays with pathogenic bacteria, necrotrophic and biotrophic fungi, as well as insect herbivore experiments, could provide valuable insights. Such work would build on existing studies that have established a causal link between PP-InsPs and plant defense (Laha *et al.*, 2015, 2016; Gulabani *et al.*, 2022). Particularly noteworthy is the recent discovery that fungal effector proteins exhibit 5-InsP$_7$ pyrophosphatase activity (McCombe *et al.*, 2023), along with activities against 4-InsP$_7$, 6-InsP$_7$, and partially 1-InsP$_7$, but not 3-InsP$_7$ (Figure 11). As proposed by Combe and colleagues (2023), these effectors might simply be employed to induce PSR at the expense of plant defense. Alternatively, a change in 4/6-InsP$_7$may also play a direct role in suppressing plant defenses, a topic deserving further investigation.

We also observed differential expression of a number of Fe-regulated genes in the mutant lines (Table S4). For instance *IRONMAN 3*, which encodes a peptide that activates iron deficiency response genes, as well as the gene encoding the Iron-Responsive Protein 6 *IRP6* (Hirayama *et al.*, 2018; Grillet *et al.*, 2018) were both strongly upregulated. We wonder if this response might have been triggered by cytoplasmic chelation of iron by 1/3-InsP$_7$ or 5-InsP$_7$, leading to increased expression of both Fe-deficiency-induced genes. Supporting this hypothesis, we also found downregulation of *ZAT6* and *ZAT10*, which encodes a zinc finger transcription factor that activates phytochelatin synthesis. Phytochelatins are small, cysteine-rich peptides located in the cytoplasm that primarily function to chelate and detoxify heavy metals. If Fe (and other di- or trivalent metals) are chelated by increased cytoplasmic PP-InsPs, it is conceivable that phytochelatin expression would decrease, as the need for metal detoxification might be reduced. In addition, *FER1*, encoding the Fe storage protein ferritin (Briat *et al.*, 2010), was downregulated as well, in agreement with a potentially reduced (cytoplasmic) availability of Fe and thus compromised Fe sensing (Table S4). This disturbance in iron homeostasis might also explain why subclade II *nudt12/13/16* plants display decreased shoot Fe content (Figure 7B). Alternatively, disturbed Fe homeostasis might also be a consequence of altered PP-InsP signaling in these mutants, topics warranting further investigation in future studies.

Material and methods

Plant materials and growth conditions

Seeds of *Arabidopsis thaliana* WT (Col-0) and T-DNA insertion lines *nudt4-1* (SALK_102051.27.90.x), *nudt4-2* (SAIL_1211_A06), *nudt17-1* (SAIL_500_D10), *nudt18-1* (SALKseq_117563.1), *nudt21-1* (SALK_031788.56.00.x), *nudt21-2* (SALKseq_132932.101) and *mrp*5 (GK-068B10) were obtained from The European Arabidopsis Stock Centre (http://arabidopsis.info/). To identify homozygous mutant lines, the plants were genotyped by PCR using the primers indicated in Table S5.

For sterile growth, *Arabidopsis thaliana* seeds were surface sterilized by washing them three times with 70 % (v/v) ethanol mixed with 0.05 % (v/v) Triton X-100 and once with 100 % (v/v) ethanol. Sterilized seeds were sown onto ½ MS (Murashige and Skoog 1962) plates containing 0.5 % (w/v) sucrose and 0.7 % (w/v) Phytagel (Sigma-Aldrich), pH 5.7. The seeds were stratified for 2 days at 4 °C and afterwards transferred to a growth chamber with a 16 h/8 h day/night period and a temperature of 22 °C/20 °C to amplify seeds.

For the affinity pull-down with the 5-PCP-InsP_5 resin, the plants were grown for 3 weeks in a growth incubator (Percival) with an 8 h/16 h day/night period and a temperature of 22 °C/20 °C. The roots and shoots of approximately 150 seedlings were collected and frozen in liquid nitrogen.

For the quantification of inositol pyrophosphate content by CE-ESI-MS, the control and mutant lines were grown on ½ MS plates. After 14 days, the shoots were collected and transferred to 2 mL centrifuge tubes and frozen in liquid nitrogen. The remaining plant material from the plates was transferred to pots containing peat substrate (Einheitserde Vermehrungserde) in block randomized design, and plants were grown for another week. 100 mg material was harvested and frozen in liquid nitrogen. The material was later grinded into powder and used for RNA extraction.

For nutrient content analyses, WT and triple mutant plants were grown for 4 weeks in pots containing peat-based substrate (Einheitserde Vermehrungserde) in block randomized design. The whole shoots were harvested and dried at 60 °C for 5 days, grinded into fine powder and the nutrient content was analyzed using ICP-OES.

To investigate the P_i-dependent regulation of inositol (pyro)phosphates, the Arabidopsis plants were hydroponically grown as described previously (Riemer *et al.*, 2021).

Constructs

The open reading frames (ORFs) of *NUDT4* (At1g18300), *NUDT7* (At4g12720), *NUDT12* (At1g12880), *NUDT13* (At3g26690), *NUDT16.1* (At3g12600.1), *NUDT16.2* (At3g12600.2), *NUDT17* (At2g01670), *NUDT18* (At1g14860), *NUDT21* (At1g73540) were amplified from *Arabidopsis thaliana* seedling cDNA by PCR, fused to Gateway compatible *attB*1 and *att*B2 sites with primers listed in Table S5 and cloned in pDONR221 (Invitrogen) with BP clonase II (Invitrogen) following the manufacturer's instructions. To express recombinant proteins fused N-terminally to a His_6-maltose-binding protein (MBP) epitope tag, the ORFs were recombined into the bacterial expression vector pDest-566 (Addgene plasmid #11517 was a gift from Dominic Esposito; http://n2t.net/addgene:11517 ; RRID:Addgene_11517) by LR clonase II (Invitrogen) following the manufacturer's instructions. His-tagged MBP used as control for the *in vitro* assays was expressed with a modified pET28b vector encoding a His_8-MBP protein (Laha *et al.*, 2015). His_8-MBP-VIH2 and His_8-MBP-hsITPK were expressed with the previously mentioned modified pETB28b vector (Laha *et al.*, 2015, 2019).

The fungal NUDT genes *MoNUDT*, *CgNUDT*, *ChNUDT* and *CtNUDT* were ordered in a pTWIST ENTR vector (Twist Biosciences, San Francisco, CA, USA). The ORFs were then recombined into the bacterial expression vector pDest-527 (Addgene plasmid #11518 was a gift from Dominic Esposito; http://n2t.net/addgene:11518 ; RRID:Addgene_11518) by LR clonase II (Invitrogen) following the manufacturer's instructions.

For the *RUBY*-reporter construct, 1 kb *SlSPX2* promoter was fused upstream of the *RUBY* reporter. The given *SlSPX2*promoter-*RUBY* fusion was placed in a LII α (4-5) plasmid backbone.

For yeast expression, the tested NUDTs were translationally fused with a C-terminal V5 epitope tag (primers listed in Table S5). The amplified genes harboring the *V5* sequence were cloned with BP clonase II in pDONR221 and then recombined into the destination vector pAG425GPD-*ccdB* (Alberti *et al.*, 2007)(Addgene plasmid #14154 was a gift from Susan Lindquist; http://n2t.net/addgene:14154; RRID:Addgene_14154) with LR clonase II following the manufacturer's instructions.

Generation of high order NUDT mutants in plants with CRISPR/Cas9

CRISPR-Cas9 constructs were generated as described earlier (Ursache *et al.*, 2021), with sgRNAs listed in Table S6. For each of the *nudt4/nudt17/nudt18/nudt21* quadruple and the *nudt12/nudt13/nudt16* triple mutants, two constructs were generated: one with the *sgRNA-NUDT17.1*, *sgRNA-NUDT18.2*, *sgRNA-NUDT21.1* and *sgRNA-NUDT4.2* in the expression vector pRU295 (Addgene plasmid #167694 was a gift from Niko Geldner;

http://n2t.net/addgene:167694; RRID:Addgene_167694), and one construct with *sgRNA-NUDT18.1*, *sgRNA-NUDT17.2*, *sgRNA-NUDT4.1* and *sgRNA-NUDT21.2* in the expression vector pRU294 (Addgene plasmid #16768 was a gift from Niko Geldner; http://n2t.net/addgene:167689; RRID:Addgene_167689). To generate the triple mutant, *sgRNA-NUDT12.1*, *sgRNA-NUDT13.2*, *sgRNA-NUDT16.1* and *sgRNA-NUDT16.2* were cloned in the expression vector pRU295 and sgRNA-*NUDT13.1* and *sgRNA-NUDT12.2* were cloned in the expression vector pRU294.

The triple *nudt12/nudt13/nudt16* and quadruple *nudt4/nudt17/nudt18/nudt21* mutants were then generated by co-transforming *Arabidopsis thaliana* WT plants with *Agrobacterium tumefaciens* strain GV3101 harboring the respective pRU294 or pRU295 constructs. By co-transforming the plants, it was possible to insert CRISPR-Cas9 constructs targeting two specific sequences for each NUDT. The plants were transformed twice with the floral dip method (Clough & Bent, 1998). Three days after the first infiltration, the plants were transformed again to increase the transformation efficiency.

The seeds were screened for a red and green fluorescence signal using a fluorescent stereomicroscope. The seeds were sterilized and germinated on ½ MS plates as described before. After two weeks, the seedlings were separated in pots and plant gDNA was extracted from leaves with the Phire Plant Direct PCR kit (Thermo Fisher). The promoter and gene regions of the targeted genes were amplified with the primers listed in Table S5 and analyzed by Sanger Sequencing.

Yeast strains, transformation and growth

The BY4741 WT (MATa *his*3Δ *leu*2Δ *met*15Δ *ura*3Δ) and *ddp1Δ* (MATa *his*3Δ *leu*2Δ *met*15Δ *ura*3Δ *ddp1Δ::KanMX*) were obtained from Euroscarf. The yeast cells were transformed with the Li-acetate method (Gietz *et al.*, 1995) and grown on 2x CSM-Leu plates for 3 days at 28 °C. Yeast transformants were grown in the respective media overnight at 28 °C in a rotating wheel before radioactive labeling with [^{3}H]-*myo*-inositol.

Affinity pull-down with 5PCP-InsP$_5$ resin

The plant material was powdered with mortar and pestle. 3 mL of lysis buffer (50 mM Tris pH 7.5, 100 mM NaCl, 5 mM ß-mercaptoethanol, 1 mM $MgCl_2$, 0.1 % Tween 20, 10 % glycerol and cOmplete™ ULTRA EDTA free protease inhibitor tablets (Roche, Basel, Switzerland)) was added to the ground shoots and 1 mL was added to the ground roots. The suspension was pelleted at 4 °C for 15 min at 19000 x g and the supernatant was transferred to a new tube

and centrifuged again. The resulting extract was filtered through a 20 µm syringe filter to remove remaining particles.

A 200 µL suspension of 5-PCP-$InsP_5$ beads or control beads was washed three times for 5 min in 50 mM Tris pH 7.5, 100 mM NaCl, 1 mM $MgCl_2$, 10 % glycerol (Wu *et al.*, 2016). After equilibration, the beads were incubated with the prepared plant lysates for 2 h at 4 °C on an overhead shaker. The beads were then rinsed three times for 10 min with the equilibration buffer and then washed overnight at 4 °C with 100 µL $InsP_6$-containing wash buffer (50 mM Tris, 100 mM NaCl, 1 mM $MgCl_2$, 20 mM $InsP_6$ (SiChem) on a rotating shaker. Afterwards, beads were pelleted and rinsed again with 50 µL of wash buffer for 10 min. The beads were then further analyzed by LC-MS/MS.

$InsP_6$-washed beads were submitted to an on-bead digestion. In brief, dry beads were re-dissolved in 50 µL digestion buffer 1 (50 mM Tris, pH 7.5, 2 M urea, 1 mM DTT), trypsin (125 ng) was added and beads were incubated for 30 min at 30 °C in a thermal shaker with 400 rpm. Next, beads were pelleted and the supernatant was transferred to a fresh tube. Digestion buffer 2 (50 mM Tris, pH 7.5, 2 M urea, 5 mM CAA) was added to the beads and mixed, beads were pelleted and the supernatant was collected and combined with the previous one. The combined supernatants were then incubated overnight at 32 °C in a thermal shaker with 400 rpm. Samples were protected from light during incubation. The digestion was stopped by adding 1 µL TFA and desalted with C18 Empore disk membranes according to the StageTip protocol. The proteins that were eluted with an excess of $InsP_6$ were reduced with dithiothreitol (DTT), alkylated with chloroacetamide (CAA), and digested with trypsin. These digested samples were desalted using StageTips with C18 Empore disk membranes (3 M), dried in a vacuum evaporator, and dissolved in 2 % ACN, 0.1 % TFA (Rappsilber *et al.*, 2003).

Dried peptides were re-dissolved in 2 % ACN, 0.1 % TFA (10 µL) for analysis. Samples were analyzed using an EASY-nLC 1000 (Thermo Fisher) coupled to a Q Exactive mass spectrometer (Thermo Fisher). Peptides were separated on 16 cm frit-less silica emitters (New Objective, 0.75 µm inner diameter) and packed in-house with reversed-phase ReproSil-Pur C18 AQ 1.9 µm resin (Dr. Maisch). Peptides were loaded on the column and eluted for 115 min using a segmented linear gradient of 5 % to 95 % solvent B (0 min : 5 % B; 0 - 5 min -> 5 % B; 5 - 65 min -> 20 % B; 65 - 90 min ->35 % B; 90 - 100 min -> 55 % B; 100 - 105 min -> 95 % B, 105-115 min -> 95 % B) (solvent A 0 % ACN, 0.1 % FA; solvent B 80 % ACN, 0.1 % FA) at a flow rate of 300 nL/min. Mass spectra were acquired in data-dependent acquisition mode with a TOP15 method. MS spectra were acquired in the Orbitrap analyzer with a mass range of 300–1750 m/z at a resolution of 70,000 FWHM and a target value of 3×106 ions. Precursors were selected with an isolation window of 2.0 m/z. HCD fragmentation was

performed at a normalized collision energy of 25. MS/MS spectra were acquired with a target value of 105 ions at a resolution of 17,500 FWHM, a maximum injection time (max.) of 55 ms and a fixed first mass of m/z 100. Peptides with a charge of +1, greater than 6, or with unassigned charge state were excluded from fragmentation for MS2, dynamic exclusion for 30 s prevented repeated selection of precursors.

Raw data were processed using MaxQuant software (version 1.5.7.4, http://www.maxquant.org/) (Cox & Mann, 2008) with label-free quantification (LFQ) and iBAQ enabled (Tyanova *et al.*, 2016) and the match-between runs option disabled. MS/MS spectra were searched by the Andromeda search engine against a combined database containing the sequences from *A. thaliana* (TAIR10_pep_20101214; ftp://ftp.arabidopsis.org/home/tair/Proteins/TAIR10_protein_lists/) and sequences of 248 common contaminant proteins and decoy sequences. Trypsin specificity was required and a maximum of two missed cleavages allowed. Minimal peptide length was set to seven amino acids. Carbamidomethylation of cysteine residues was set as fixed, oxidation of methionine and protein N-terminal acetylation as variable modifications. Peptide-spectrum-matches and proteins were retained if they were below a false discovery rate of 1 %.

The MaxQuant output (msms.txt) was further processed using Skyline (https://skyline.ms) (MacLean *et al.*, 2010). Peaks were inspected and, if necessary, re-integrated manually. To identify potential binding candidates, proteins were filtered for two or more unique peptides and idot products with > 0.95 confidence. Subsequently, peptides were assessed individually for enrichment in the 5-PCP-InsP_5 condition versus the control condition based on peak areas. Background binders were identified as proteins with equal abundance in both the 5-PCP-InsP_5 and control conditions.

ICP-OES analyses

Shoots of 4-week-old plants were dried, ground to powder and 0.150 g were digested with 3 mL nitric acid (HNO_3, 65 %) in a microwave-accelerated reaction system (CEM, Matthews, NC, USA). Nutrient concentrations were measured using inductively coupled plasma optical emission spectroscopy (ICP-OES; iCAP Pro X ICP-OES Duo; Thermo Fisher Scientific, Waltham, MA, USA). To ensure precision and accuracy throughout the analyses standard materials (IPE100; Wageningen Evaluation Programs for Analytical Laboratories, WEPAL; Wageningen University, the Netherlands) were used.

Protein preparation

Recombinant NUDT proteins fused to His_6-MBP and free His_8-MBP protein were expressed in *E. coli* BL21-CodonPlus(DE3)-RIL cells (Stratagene). The bacterial cultures were grown overnight and fresh 2YT medium (16 g/L tryptone, 10 g/L yeast extract, 5 g/L NaCl) with respective antibiotics was inoculated 1:500 with the overnight culture. In the case of CgNUDT and ChNUDT LB Medium (10 g/L tryptone, 5 g/L yeast extract, 10 g/L NaCl) and in the case of CtNUDT TB medium (12 g/L tryptone, 24 g/L yeast extract, 0.4 % v/v glycerol, 0.017 M KH_2PO_4, 0.072 K_2HPO_4) was used. The cultures were grown for 3 h at 37 °C while shaking (200 rpm) to reach an estimated OD_{600} of 0.6. Protein expression was induced by adding 0.1 mM (CgNUDT, ChNUDT, CtNUDT), 0.125 mM (NUDT7 and -12), 0.25 mM (NUDT4, -16, -17, -18, and -21) or 0.5 mM (NUDT13, MoNUDT) isopropyl-d-1-thiogalactopyranoside (IPTG). The cultures were grown for 24 h at 12 °C (NUDT4, and -18) or at 16 °C (NUDT7, -13, -16, -17, and -21, CgNUDT, ChNUDT) or for 3 h at 37 °C (NUDT12, MoNUDT, CtNUDT). Bacterial cells were lysed by vortexing the cells 8 times for 1 min with lysis buffer (20 mM Na_2HPO_4, 300 mM NaCl, 2 mM DTT, 0.05 mM EDTA and 1 % Triton X-100, pH 7.4) and glass beads (0.1 – 0.25 mm). NUDT4, -17, -18, and -21 were purified using a FPLC (ÄKTA pure™), while NUDT12, -13, -16, MoNUDT, CgNUDT, ChNUDT and CtNUDT were batch purified using Ni-NTA agarose resin (Macherey-Nagel). For both methods, the same binding buffer (20 mM Na_2HPO_4, 500 mM NaCl, 25 mM Imidazol, pH 7.4) and elution buffer (20 mM Na_2HPO_4, 500 mM NaCl, 500 mM Imidazol, pH 7.4) were used. The recombinant proteins were concentrated and imidazole was diluted by using Vivaspin 20 (50 kDa, Merck) for FPLC-purified proteins or Amicon Ultra 0.5 mL Centrifugal Filters (50 kDa, Merck) for the batch-purified proteins and the elution buffer without imidazole. The purified proteins were mixed with 20 % glycerol and stored at -20 °C. Recombinant Arabidopsis and human ITPK1 and VIH2 proteins fused to His_8-MBP were expressed and purified as described before (Laha *et al.*, 2015, 2019). Concentrations were estimated by using SDS-PAGE followed by Coomassie blue staining and comparing the proteins with designated amounts of a BSA standard.

In vitro (PP-)InsP assays

The (PP-)InsP pyrophosphatase assays were performed with recombinant His_6-MBP-NUDT proteins or His_8-MBP proteins as control and 50 mM HEPES (pH 7.0), 10 mM NaCl, 5 % (v/v) glycerol, 0.1 % (v/v) β-mercaptoethanol, either 1 mM EDTA, $MnCl_2$, $MgCl_2$, $CaCl_2$, or $ZnCl_2$ and 0.33 mM of various $InsP_7$ or $InsP_8$ isomers as indicated. The recombinant protein concentrations were: ~4.9 µM His_6-MBP-NUDT4, ~3.7 µM His_6-MBP-NUDT12, ~1.9 µM His_6-MBP-NUDT13, ~0.6 µM His_6-MBP-NUDT16.1, ~15.8 µM His_6-MBP-NUDT16.2, ~2.0 µM His_6-

MBP-NUDT17, ~5.1 µM His_6-MBP-NUDT18 and ~5.0 µM His_6-MBP-NUDT21. For the assays with His_6-MBP-MoNUDT, His_6-MBP-CgNUDT, His_6-MBP-ChNUDT and His_6-MBP-CtNUDT 0.25 mM of the various $InsP_7$ isomers and 0.13 µg/µL protein was used.

PP-InsP pyrophosphatase assays with higher subclade II protein concentrations were performed with ~7 µM His_6-MBP-NUDT7, ~7.5 µM His_6-MBP-NUDT12 or His_6-MBP-NUDT13, and ~8 µM His_6-MBP-NUDT16.1 or His_6-MBP-NUDT16.2. The pyrophosphatase assays with a higher subclade I protein concentration were performed in a reaction buffer as described previously (Riemer *et al.*, 2021) with 0.33 mM of various $InsP_7$ or $InsP_8$ isomers as indicated. The recombinant protein concentrations were ~9 µM His_6-MBP-NUDT4, ~6 µM His_6-MBP-NUDT17, ~6 µM His_6-MBP-NUDT18 and ~8 µM His_6-MBP-NUDT21. $InsP_7$ and $InsP_8$ isomers were chemically synthesized as described previously (Capolicchio *et al.*, 2013, 2014). The reactions were incubated for 1 h at 28 °C or 2 h at 22 °C and either separated by 33 % PAGE and visualized by toluidine blue staining or analyzed by CE-ESI-MS as described previously (Qiu *et al.*, 2020; Riemer *et al.*, 2021). Kinase assays were performed as described previously (Riemer *et al.*, 2021) with 0.2 µg/µl of protein.

Inositol phosphate extraction and purification

The extraction and purification of inositol phosphates of *Arabidopsis thaliana* T-DNA insertion lines were performed using TiO_2 (titanium(IV) oxide rutile, Sigma Aldrich) beads as previously described in (Riemer *et al.*, 2021). Inositol phosphate from the triple mutant *nudt12/13/16*, quadruple mutant *nudt4/17/18/21* and *N. benthamiana* were extracted with Nb_2O_5 beads (Niobium (V) pentoxide, Sigma Aldrich) as described in the following. The beads were weighted to 20 mg for each sample and washed once in water (300 µL) and once in 1 M perchloric acid (300 µL) (PA). Liquid N_2-frozen plant material was homogenized using a pestle and immediately resuspended in 800 µL ice-cold PA (1 M). Samples were kept on ice for 10 min with short intermediate vortexing and then centrifuged for 10 min at 18000 g at 4 °C. The supernatants were transferred into fresh 1.5-mL tubes and centrifuged again for 10 min at 18000 g at 4 °C. To bind InsPs onto the beads, the supernatants were resuspended in the prewashed Nb_2O_5 beads and rotated at 4 °C for 45 min. Afterwards, the tubes were centrifuged at 11000 g for 1 min at 4 °C and washed twice in 500 µL ice-cold PA (1 M) and once with 500 µL PA (0.1 M). To elute inositol polyphosphates, beads were resuspended in 200 µL 10 % ammonium hydroxide and then rotated for 5 min at room temperature. After centrifuging, the supernatants were transferred into fresh 1.5-mL tubes. The elution process was repeated and the second supernatants were added to the first. Eluted samples were vacuum evaporated at 45 °C to dry completely.

PAGE, CE-ESI-MS and HPLC analyses

Arabidopsis plants and yeast transformants were radioactively labeled with [^{3}H]-*myo*-inositol (ARC), extracted and analyzed via SAX-HPLC as described before (Azevedo & Saiardi, 2006; Laha *et al.*, 2015; Gaugler *et al.*, 2020). *In vitro* biochemical assays were analyzed by PAGE and CE-ESI-MS, and purified inositol phosphates of *A. thaliana* mutant lines or *N. benthamiana* leaves were analyzed by CE-ESI-MS as described in (Qiu *et al.*, 2023; Qiu *et al.*, 2020; Riemer *et al.*, 2021).

RNA extraction and quantitative real-time PCR

Total RNA was extracted from homogenized root or shoot samples using the NucleoSpin RNA Mini Kit (Machery-Nagel), followed by on-column DNase treatment (QIAGEN), according to the manufacturers' protocols. cDNA was synthesized from 0.5-1 µg RNA by reverse transcription using the RevertAid First Strand cDNA synthesis Kit (Thermo Fisher Scientific) and oligo(dT) primer. A ten- or twenty-times diluted cDNA sample was then used for quantitative real-time (RT) PCR analysis with the CFX384 Touch Real-Time PCR Detection System (Bio-Rad Laboratories) and the iQ SYBR Green Supermix (Bio-Rad Laboratories). All reactions were repeated in two technical and three biological replicates. Recorded C_t values were exported from the Bio-Rad CFX Manager Software (Version 3.1, Bio-Rad Laboratories) and used for the calculation of relative expression values according to $\Delta\Delta$CT method and using *UBQ2* (*At2g36170*) or *ACTIN2* (*At3g18780*) as the reference gene. The reactions were carried out using the primers listed in Table S5.

Total RNA for transcriptome analysis was extracted from shoot samples using the QIAGEN Kit followed by on-column DNase treatment (QIAGEN), according to the manufacturers' protocols.

RNA sequencing, bioinformatic analysis and data visualization

For RNA-seq analysis, total RNA was extracted as mentioned above. Library construction and sequencing were performed at BGI Genomics (Poland). mRNA enrichment was performed on total RNA using oligo(dT)-attached magnetic beads. The enriched mRNA with poly(A) tails was fragmented using a fragmentation buffer, followed by reverse transcription using random N6 primers to synthesize cDNA double strands. The synthesized double-stranded DNA was then end-repaired and 5'-phosphorylated, with a protruding 'A' at the 3' end forming a blunt end, followed by ligation of a bubble-shaped adapter with a protruding 'T' at the 3' end. The ligation products were PCR amplified using specific primers. The PCR products were denatured to

single strands, and then single-stranded circular DNA libraries were generated using abridged primer. The constructed libraries were quality-checked and sequenced after passing the quality control. Sequencing was performed on the DNBSEQ platform using paired-end 150 bp reads(PE150). The raw data obtained from sequencing were filtered using SOAPnuke (Chen *et al.*, 2017) to remove adapters, reads containing ploy-N and low-quality reads, the filtered data (clean reads) were aligned to the Arabidopsis genome (TAIR10) using HISAT (Kim *et al.*, 2015) based on Burrows-Wheeler transform and Ferragina-Manzini (FM) index. Clean data was aligned to the reference gene set using Bowtie2 (v2.3.4.3) (Langmead & Salzberg, 2012). Gene expression quantification was performed using RSEM (v1.3.1) (Li & Dewey, 2011) software, and gene expression clustering heatmaps across different samples were generated using pheatmap (v1.0.8) (Kolde, Raivo, 2010). DESeq2 (v1.4.5) (Love *et al.*, 2014) (orDEGseq (Wang *et al.*, 2010) or PoissonDis (Audic & Claverie, 1997)) was employed for differential gene (DEGs) detection, with criteria set as Q (Storey *et al.*, 2024) value < 0.05 or FDR ≤ 0.001 and (|log2FC| > 1). The subsequent analysis and data mining were performed on Dr. Tom Multi-omics Data mining system (https://biosys.bgi.com).

For the GO terms (http://www.geneontology.org/), the base mean expression for each gene was calculated as the average expression of mutant and control samples (base mean = (avg. Exp. of Mutant + avg. Exp of Control) / 2). Genes with a base mean greater than 20 were selected to form the background set. From this background, an interest set was defined by selecting genes with a log2 fold change (|log2FC| > 1), and Q-values < 0.05. GO enrichment analysis was performed using the topGO (Alexa & Rahnenfuhrer, 2024) package for all three gene ontology categories: biological process (BP), cellular component (CC), and molecular function (MF). The weigh01 algorithm and Fisher's exact test were employed as parameters, and the results were filtered to include the top 200 GO terms (nodes). The significance of each GO term was represented by the p-value, and the top 10 GO terms were plotted, ordered by p-value. Data manipulation (Wickham *et al.*, 2019, 2023) and visualization (Hadley Wickham, 2016; Wilke, 2024) for GO terms was done in R software (R Core Team, 2023). Go enrichment bubble chart was done using the hypergeometric test implemented in Phyper function in R software, with a threshold of Q value≤ 0.05.

Tobacco growth conditions and infiltration procedure

Nicotiana benthamiana seeds were germinated in a growth chamber with a 16 h/8 h day/night period and a temperature of 22 °C/20 °C for 6 weeks prior to infiltration. A single colony of transformed *Agrobacterium tumefaciens* strain GV3101 containing T-DNA vectors was inoculated in 2 mL of YEB media containing the respective antibiotics and cultivated overnight at 28 °C while shaking. On the following day, 500 µL of overnight culture was added to 5 mL of fresh YEB with respective antibiotics and grown for another 4-6 h at 28 °C. Cultures were

harvested by centrifugation at room temperature with 4000 g for 10 min. The pellet was resuspended in 250 µL infiltration medium containing 10 mM $MgCl_2$, 10 mM MES (pH 5.8) and 150 µM Acetosyringone. OD_{600} was determined using a 1:10 dilution and adjusted to OD_{600} = 0.8 in infiltration solution. The working solution for the RUBY assay was prepared by adding equal amounts of RUBY-reporter and NUDTs strains, and adding p19 (OD_{600} = 0.05). For the working solution of the NUDT overexpression experiment, the NUDT infiltration solution was added with p19 (OD_{600} = 0.05). The mixtures were then infiltrated into the abaxial surface of 4-6-week-old *N. benthamiana* leaves using a 1 mL syringe without a needle. After infiltration, the plants were kept under previous growth conditions for 2-3 days before analyzing RUBY staining or extracting and purifying the inositol phosphates.

Acknowledgments

The authors thank Brigitte Ueberbach, Li Schlüter, Nur Gömec (Department of Plant Nutrition, Institute of Crop Science and Resource Conservation, University of Bonn), Jacqueline Fuge (Department of Physiology & Cell Biology, Leibniz-Institute of Plant Genetics and Crop Plant Research) and Anne Harzen (Plant Proteomics and Mass Spectronomy Group, Max Planck Institute for Plant Breeding Research) for excellent technical assistance.

Funding

This work was funded by grants from the Deutsche Forschungsgemeinschaft (SCHA 1274/4-1, SCHA 1274/5-1, and under Germany's Excellence Strategy, EXC-2070-390732324, PhenoRob to G.S.; JE 572/4-1 and under Germany's Excellence Strategy, CIBSS-EXC-2189-Project ID 390939984 to H.J.J.; LA 1338/18-1 to T.L.).

References

Alberti S, Gitler AD, Lindquist S. **2007**. A suite of Gateway cloning vectors for high-throughput genetic analysis in Saccharomyces cerevisiae. *Yeast (Chichester, England)* **24**: 913–919.

Alexa A, Rahnenfuhrer J. **2024**. topGO. *Bioconductor*.

Andreeva N, Ledova L, Ryazanova L, Tomashevsky A, Kulakovskaya T, Eldarov M. **2019**. Ppn2 endopolyphosphatase overexpressed in *Saccharomyces cerevisiae*: Comparison with Ppn1, Ppx1, and Ddp1 polyphosphatases. *Biochimie* **163**: 101–107.

Audic S, Claverie J-M. **1997**. The Significance of Digital Gene Expression Profiles. *Genome Research* **7**: 986–995.

Azevedo C, Saiardi A. **2006**. Extraction and analysis of soluble inositol polyphosphates from yeast. *Nature Protocols* **1**: 2416–2422.

Bessman MJ, Frick DN, O'Handley SF. **1996**. The MutT Proteins or "Nudix" Hydrolases, a Family of Versatile, Widely Distributed, "Housecleaning" Enzymes *. *Journal of Biological Chemistry* **271**: 25059–25062.

Blüher D, Laha D, Thieme S, Hofer A, Eschen-Lippold L, Masch A, Balcke G, Pavlovic I, Nagel O, Schonsky A, *et al.*2017. A 1-phytase type III effector interferes with plant hormone signaling. *Nature Communications* **8**: 2159.

Briat J-F, Duc C, Ravet K, Gaymard F. **2010**. Ferritins and iron storage in plants. *Biochimica et Biophysica Acta (BBA) - General Subjects* **1800**: 806–814.

Bustos R, Castrillo G, Linhares F, Puga MI, Rubio V, Pérez-Pérez J, Solano R, Leyva A, Paz-Ares J. **2010**. A Central Regulatory System Largely Controls Transcriptional Activation and Repression Responses to Phosphate Starvation in Arabidopsis. *PLOS Genetics* **6**: e1001102.

Capolicchio S, Thakor DT, Linden A, Jessen HJ. **2013**. Synthesis of Unsymmetric Diphospho-Inositol Polyphosphates. *Angewandte Chemie International Edition* **52**: 6912–6916.

Capolicchio S, Wang H, Thakor DT, Shears SB, Jessen HJ. **2014**. Synthesis of Densely Phosphorylated Bis-1,5-Diphospho-myo-Inositol Tetrakisphosphate and its Enantiomer by Bidirectional P-Anhydride Formation. *Angewandte Chemie International Edition* **53**: 9508–9511.

Chabert V, Kim G-D, Qiu D, Liu G, Michaillat Mayer L, Jamsheer K M, Jessen HJ, Mayer A. **2023**. Inositol pyrophosphate dynamics reveals control of the yeast phosphate starvation program through 1,5-IP8 and the SPX domain of Pho81 (C Gutjahr and D Ron, Eds.). *eLife* **12**: RP87956.

Chen Y, Chen Y, Shi C, Huang Z, Zhang Y, Li S, Li Y, Ye J, Yu C, Li Z, *et al.*2017. SOAPnuke: a MapReduce acceleration-supported software for integrated quality control and preprocessing of high-throughput sequencing data. *GigaScience* **7**: gix120.

Clough SJ, Bent AF. **1998**. Floral dip: a simplified method for -mediated transformation of. *The Plant Journal* **16**: 735–743.

Couso I, Evans BS, Li J, Liu Y, Ma F, Diamond S, Allen DK, Umen JG. **2016**. Synergism between Inositol Polyphosphates and TOR Kinase Signaling in Nutrient Sensing, Growth Control, and Lipid Metabolism in Chlamydomonas. *The Plant Cell* **28**: 2026–2042.

Cox J, Mann M. **2008**. MaxQuant enables high peptide identification rates, individualized p.p.b.-range mass accuracies and proteome-wide protein quantification. *Nature Biotechnology* **26**: 1367–1372.

Desai M, Rangarajan P, Donahue JL, Williams SP, Land ES, Mandal MK, Phillippy BQ, Perera IY, Raboy V, Gillaspy GE. **2014**. Two inositol hexakisphosphate kinases drive inositol pyrophosphate synthesis in plants. *The Plant Journal* **80**: 642–653.

Dollins DE, Bai W, Fridy PC, Otto JC, Neubauer JL, Gattis SG, Mehta KPM, York JD. **2020**. Vip1 is a kinase and pyrophosphatase switch that regulates inositol diphosphate signaling. *Proceedings of the National Academy of Sciences of the United States of America* **117**: 9356–9364.

Dong J, Ma G, Sui L, Wei M, Satheesh V, Zhang R, Ge S, Li J, Zhang T-E, Wittwer C, *et al.*2019. Inositol Pyrophosphate InsP8 Acts as an Intracellular Phosphate Signal in

Arabidopsis. *Molecular Plant* **12**: 1463–1473.
Draškovič P, Saiardi A, Bhandari R, Burton A, Ilc G, Kovačevič M, Snyder SH, Podobnik M. **2008**. Inositol Hexakisphosphate Kinase Products Contain Diphosphate and Triphosphate Groups. *Chemistry & Biology* **15**: 274–286.
Fisher DI, Safrany ST, Strike P, McLennan AG, Cartwright JL. **2002**. Nudix Hydrolases That Degrade Dinucleoside and Diphosphoinositol Polyphosphates Also Have 5-Phosphoribosyl 1-Pyrophosphate (PRPP) Pyrophosphatase Activity That Generates the Glycolytic Activator Ribose 1,5-Bisphosphate*. *Journal of Biological Chemistry* **277**: 47313–47317.
Fleet CM, Yen JY, Hill EA, Gillaspy GE. **2018**. Co-suppression of AtMIPS demonstrates cooperation of MIPS1, MIPS2 and MIPS3 in maintaining myo-inositol synthesis. *Plant Molecular Biology* **97**: 253–263.
Flores S, Smart CC. **2000**. Abscisic acid-induced changes in inositol metabolism in Spirodela polyrrhiza. *Planta* **211**: 823–832.
Fridy PC, Otto JC, Dollins DE, York JD. **2007**. Cloning and characterization of two human VIP1-like inositol hexakisphosphate and diphosphoinositol pentakisphosphate kinases. *The Journal of biological chemistry* **282**.
Furkert D, Nadler-Holly M, Fiedler D. **2021**. Affinity enrichment and identification of inositol poly- and pyrophosphate interactomes. *STAR Protocols* **2**: 100277.
Gaugler P, Gaugler V, Kamleitner M, Schaaf G. **2020**. Extraction and Quantification of Soluble, Radiolabeled Inositol Polyphosphates from Different Plant Species using SAX-HPLC. *Journal of Visualized Experiments*: 61495.
Gaugler P, Schneider R, Liu G, Qiu D, Weber J, Schmid J, Jork N, Häner M, Ritter K, Fernández-Rebollo N, *et al.*2022. Arabidopsis PFA-DSP-Type Phosphohydrolases Target Specific Inositol Pyrophosphate Messengers. *Biochemistry* **61**: 1213–1227.
Ge X, Li G-J, Wang S-B, Zhu H, Zhu T, Wang X, Xia Y. **2007**. AtNUDT7, a Negative Regulator of Basal Immunity in Arabidopsis, Modulates Two Distinct Defense Response Pathways and Is Involved in Maintaining Redox Homeostasis. *Plant Physiology* **145**: 204–215.
Gerasimaite R, Pavlovic I, Capolicchio S, Hofer A, Schmidt A, Jessen HJ, Mayer A. **2017**. Inositol Pyrophosphate Specificity of the SPX-Dependent Polyphosphate Polymerase VTC. *ACS chemical biology* **12**: 648–653.
Gietz RD, Schiestl RH, Willems AR, Woods RA. **1995**. Studies on the transformation of intact yeast cells by the LiAc/SS-DNA/PEG procedure. *Yeast (Chichester, England)* **11**: 355–360.
Grillet L, Lan P, Li W, Mokkapati G, Schmidt W. **2018**. IRON MAN is a ubiquitous family of peptides that control iron transport in plants. *Nature Plants* **4**: 953–963.
Gulabani H, Goswami K, Walia Y, Roy A, Noor JJ, Ingole KD, Kasera M, Laha D, Giehl RFH, Schaaf G, *et al.*2022. Arabidopsis inositol polyphosphate kinases IPK1 and ITPK1 modulate crosstalk between SA-dependent immunity and phosphate-starvation responses. *Plant Cell Reports* **41**: 347–363.
Gunawardana D, Likic VA, Gayler KR. **2009**. A Comprehensive Bioinformatics Analysis of the Nudix Superfamily in Arabidopsis thaliana. *International Journal of Genomics* **2009**: 820381.
Hadley Wickham. **2016**. *ggplot2: Elegant Graphics for Data Analysis | SpringerLink*. Springer Cham.
Hawkesford MJ, Cakmak I, Coskun D, De Kok LJ, Lambers H, Schjoerring JK, White PJ. **2023**. Functions of macronutrients☆. In: Rengel Z, Cakmak I, White PJ, eds. Marschner's Mineral Nutrition of Plants (Fourth Edition). San Diego: Academic Press, 201–281.
He Y, Zhang T, Sun H, Zhan H, Zhao Y. **2020**. A reporter for noninvasively monitoring gene expression and plant transformation. *Horticulture Research* **7**: 1–6.
Hirayama T, Lei GJ, Yamaji N, Nakagawa N, Ma JF. **2018**. The Putative Peptide Gene FEP1 Regulates Iron Deficiency Response in Arabidopsis. *Plant and Cell Physiology* **59**: 1739–1752.
Ishikawa K, Ogawa T, Hirosue E, Nakayama Y, Harada K, Fukusaki E, Yoshimura K,

Shigeoka S. **2009**. Modulation of the Poly(ADP-ribosyl)ation Reaction via the Arabidopsis ADP-Ribose/NADH Pyrophosphohydrolase, AtNUDX7, Is Involved in the Response to Oxidative Stress. *Plant Physiology* **151**: 741–754.
Ishikawa K, Yoshimura K, Harada K, Fukusaki E, Ogawa T, Tamoi M, Shigeoka S. **2010**. AtNUDX6, an ADP-Ribose/NADH Pyrophosphohydrolase in Arabidopsis, Positively Regulates NPR1-Dependent Salicylic Acid Signaling. *Plant Physiology* **152**: 2000–2012.
Kilari RS, Weaver JD, Shears SB, Safrany ST. **2013**. Understanding inositol pyrophosphate metabolism and function: Kinetic characterization of the DIPPs. *FEBS Letters* **587**: 3464–3470.
Kilian J, Whitehead D, Horak J, Wanke D, Weinl S, Batistic O, D'Angelo C, Bornberg-Bauer E, Kudla J, Harter K. **2007**. The AtGenExpress global stress expression data set: protocols, evaluation and model data analysis of UV-B light, drought and cold stress responses. *The Plant Journal* **50**: 347–363.
Kim D, Langmead B, Salzberg SL. **2015**. HISAT: a fast spliced aligner with low memory requirements. *Nature methods* **12**: 357.
Kim G, Liu G, Qiu D, Gopaldass N, Leo GD, Hermes J, Timmer J, Saiardi A, Mayer A, Jessen HJ. **2024**. Pools of independently cycling inositol phosphates revealed by pulse labeling with 18O-water. : 2024.05.03.592351.
Klaus SMJ, Wegkamp A, Sybesma W, Hugenholtz J, Gregory JF, Hanson AD. **2005**. A Nudix Enzyme Removes Pyrophosphate from Dihydroneopterin Triphosphate in the Folate Synthesis Pathway of Bacteria and Plants*. *Journal of Biological Chemistry* **280**: 5274–5280.
Kolde, Raivo. **2010**. pheatmap: Pretty Heatmaps. : 1.0.12.
Kuo H-F, Chang T-Y, Chiang S-F, Wang W-D, Charng Y, Chiou T-J. **2014**. Arabidopsis inositol pentakisphosphate 2-kinase, AtIPK1, is required for growth and modulates phosphate homeostasis at the transcriptional level. *The Plant Journal* **80**: 503–515.
Kuo H-F, Hsu Y-Y, Lin W-C, Chen K-Y, Munnik T, Brearley CA, Chiou T-J. **2018**. Arabidopsis inositol phosphate kinases IPK1 and ITPK1 constitute a metabolic pathway in maintaining phosphate homeostasis. *The Plant Journal: For Cell and Molecular Biology*.
Laha NP, Giehl RFH, Riemer E, Qiu D, Pullagurla NJ, Schneider R, Dhir YW, Yadav R, Mihiret YE, Gaugler P, *et al.*2022. INOSITOL (1,3,4) TRIPHOSPHATE 5/6 KINASE1-dependent inositol polyphosphates regulate auxin responses in Arabidopsis. *Plant Physiology* **190**: 2722–2738.
Laha D, Johnen P, Azevedo C, Dynowski M, Weiß M, Capolicchio S, Mao H, Iven T, Steenbergen M, Freyer M, *et al.*2015. VIH2 Regulates the Synthesis of Inositol Pyrophosphate $InsP_8$ and Jasmonate-Dependent Defenses in Arabidopsis. *The Plant Cell* **27**: 1082.
Laha D, Parvin N, Dynowski M, Johnen P, Mao H, Bitters ST, Zheng N, Schaaf G. **2016**. Inositol Polyphosphate Binding Specificity of the Jasmonate Receptor Complex. *Plant Physiology* **171**: 2364–2370.
Laha D, Parvin N, Hofer A, Giehl RFH, Fernandez-Rebollo N, von Wirén N, Saiardi A, Jessen HJ, Schaaf G. **2019**. Arabidopsis ITPK1 and ITPK2 Have an Evolutionarily Conserved Phytic Acid Kinase Activity. *ACS chemical biology* **14**: 2127–2133.
Langmead B, Salzberg SL. **2012**. Fast gapped-read alignment with Bowtie 2. *Nature Methods* **9**: 357–359.
Lee Y-S, Mulugu S, York JD, O'Shea EK. **2007**. Regulation of a cyclin-CDK-CDK inhibitor complex by inositol pyrophosphates. *Science (New York, N.Y.)* **316**: 109–112.
Lemtiri-Chlieh F, MacRobbie EAC, Brearley CA. **2000**. Inositol hexakisphosphate is a physiological signal regulating the K+-inward rectifying conductance in guard cells. *Proceedings of the National Academy of Sciences of the United States of America* **97**: 8687–8692.
Li B, Dewey CN. **2011**. RSEM: accurate transcript quantification from RNA-Seq data with or without a reference genome. *BMC Bioinformatics* **12**: 323.
Li X, Gu C, Hostachy S, Sahu S, Wittwer C, Jessen HJ, Fiedler D, Wang H, Shears SB. **2020**. Control of XPR1-dependent cellular phosphate efflux by InsP8 is an exemplar for functionally-exclusive inositol pyrophosphate signaling. *Proceedings of the National*

Academy of Sciences of the United States of America **117**: 3568–3574.
Lin H, Fridy PC, Ribeiro AA, Choi JH, Barma DK, Vogel G, Falck JR, Shears SB, York JD, Mayr GW. **2009**. Structural Analysis and Detection of Biological Inositol Pyrophosphates Reveal That the Family of VIP/Diphosphoinositol Pentakisphosphate Kinases Are 1/3-Kinases. *The Journal of Biological Chemistry* **284**: 1863–1872.
Liu F, Wang Z, Ren H, Shen C, Li Y, Ling H-Q, Wu C, Lian X, Wu P. **2010**. OsSPX1 suppresses the function of OsPHR2 in the regulation of expression of OsPT2 and phosphate homeostasis in shoots of rice. *The Plant Journal* **62**: 508–517.
Lonetti A, Szijgyarto Z, Bosch D, Loss O, Azevedo C, Saiardi A. **2011**. Identification of an Evolutionarily Conserved Family of Inorganic Polyphosphate Endopolyphosphatases. *Journal of Biological Chemistry* **286**: 31966–31974.
Losito O, Szijgyarto Z, Resnick AC, Saiardi A. **2009**. Inositol Pyrophosphates and Their Unique Metabolic Complexity: Analysis by Gel Electrophoresis. *PLOS ONE* **4**: e5580.
Love MI, Huber W, Anders S. **2014**. Moderated estimation of fold change and dispersion for RNA-seq data with DESeq2. *Genome Biology* **15**: 550.
Luo Y, Qin G, Zhang J, Liang Y, Song Y, Zhao M, Tsuge T, Aoyama T, Liu J, Gu H, *et al.*2011. d-myo-Inositol-3-Phosphate Affects Phosphatidylinositol-Mediated Endomembrane Function in Arabidopsis and Is Essential for Auxin-Regulated Embryogenesis[W][OA]. *The Plant Cell* **23**: 1352–1372.
Lv Q, Zhong Y, Wang Y, Wang Z, Zhang L, Shi J, Wu Z, Liu Y, Mao C, Yi K, *et al.*2014. SPX4 Negatively Regulates Phosphate Signaling and Homeostasis through Its Interaction with PHR2 in Rice. *The Plant Cell* **26**: 1586–1597.
MacDonald GK, Bennett EM, Potter PA, Ramankutty N. **2011**. Agronomic phosphorus imbalances across the world's croplands. *Proceedings of the National Academy of Sciences* **108**: 3086–3091.
MacLean B, Tomazela DM, Shulman N, Chambers M, Finney GL, Frewen B, Kern R, Tabb DL, Liebler DC, MacCoss MJ. **2010**. Skyline: an open source document editor for creating and analyzing targeted proteomics experiments. *Bioinformatics* **26**: 966–968.
Maruta T, Ogawa T, Tsujimura M, Ikemoto K, Yoshida T, Takahashi H, Yoshimura K, Shigeoka S. **2016**. Loss-of-function of an Arabidopsis NADPH pyrophosphohydrolase, AtNUDX19, impacts on the pyridine nucleotides status and confers photooxidative stress tolerance. *Scientific Reports* **6**: 37432.
Maruta T, Yoshimoto T, Ito D, Ogawa T, Tamoi M, Yoshimura K, Shigeoka S. **2012**. An Arabidopsis FAD Pyrophosphohydrolase, AtNUDX23, is Involved in Flavin Homeostasis. *Plant and Cell Physiology* **53**: 1106–1116.
McCombe CL, Wegner A, Zamora CS, Casanova F, Aditya S, Greenwood JR, Wirtz L, Paula S de, England E, Shang S, *et al.*2023. Plant pathogenic fungi hijack phosphate starvation signaling with conserved enzymatic effectors. : 2023.11.14.566975.
Menniti FS, Miller RN, Putney JW, Shears SB. **1993**. Turnover of inositol polyphosphate pyrophosphates in pancreatoma cells. *The Journal of Biological Chemistry* **268**: 3850–3856.
Mulugu S, Bai W, Fridy PC, Bastidas RJ, Otto JC, Dollins DE, Haystead TA, Ribeiro AA, York JD. **2007**. A Conserved Family of Enzymes That Phosphorylate Inositol Hexakisphosphate. *Science* **316**: 106–109.
Muñoz FJ, Baroja-Fernández E, Morán-Zorzano MT, Alonso-Casajús N, Pozueta-Romero J. **2006**. Cloning, Expression and Characterization of a Nudix Hydrolase that Catalyzes the Hydrolytic Breakdown of ADP-glucose Linked to Starch Biosynthesis in Arabidopsis thaliana. *Plant and Cell Physiology* **47**: 926–934.
Ogawa T, Ishikawa K, Harada K, Fukusaki E, Yoshimura K, Shigeoka S. **2009**. Overexpression of an ADP-ribose pyrophosphatase, AtNUDX2, confers enhanced tolerance to oxidative stress in Arabidopsis plants. *The Plant Journal* **57**: 289–301.
Ogawa T, Ueda Y, Yoshimura K, Shigeoka S. **2005**. Comprehensive Analysis of Cytosolic Nudix Hydrolases in *Arabidopsis thaliana**. *Journal of Biological Chemistry* **280**: 25277–25283.
Ogawa T, Yoshimura K, Miyake H, Ishikawa K, Ito D, Tanabe N, Shigeoka S. **2008**. Molecular Characterization of Organelle-Type Nudix Hydrolases in Arabidopsis. *Plant*

Physiology **148**: 1412–1424.
Osorio MB, Ng S, Berkowitz O, De Clercq I, Mao C, Shou H, Whelan J, Jost R. **2019**. SPX4 Acts on PHR1-Dependent and -Independent Regulation of Shoot Phosphorus Status in Arabidopsis. *Plant Physiology* **181**: 332–352.
Pascual-Ortiz M, Saiardi A, Walla E, Jakopec V, Künzel NA, Span I, Vangala A, Fleig U. **2018**. Asp1 Bifunctional Activity Modulates Spindle Function via Controlling Cellular Inositol Pyrophosphate Levels in *Schizosaccharomyces pombe*. *Molecular and Cellular Biology* **38**: e00047-18.
Pipercevic J, Kohl B, Gerasimaite R, Comte-Miserez V, Hostachy S, Müntener T, Agustoni E, Jessen HJ, Fiedler D, Mayer A, *et al.*2023. Inositol pyrophosphates activate the vacuolar transport chaperone complex in yeast by disrupting a homotypic SPX domain interaction. *Nature Communications* **14**: 2645.
Puga MI, Mateos I, Charukesi R, Wang Z, Franco-Zorrilla JM, de Lorenzo L, Irigoyen ML, Masiero S, Bustos R, Rodríguez J, *et al.*2014. SPX1 is a phosphate-dependent inhibitor of Phosphate Starvation Response 1 in Arabidopsis. *Proceedings of the National Academy of Sciences of the United States of America* **111**: 14947–14952.
Qi W, Manfield IW, Muench SP, Baker A. **2017**. AtSPX1 affects the AtPHR1-DNA-binding equilibrium by binding monomeric AtPHR1 in solution. *The Biochemical Journal* **474**: 3675–3687.
Qin N, Li L, Ji X, Pereira R, Chen Y, Yin S, Li C, Wan X, Qiu D, Jiang J, *et al.*2023. Flux regulation through glycolysis and respiration is balanced by inositol pyrophosphates in yeast. *Cell* **186**: 748-763.e15.
Qiu D, Gu C, Liu G, Ritter K, Eisenbeis VB, Bittner T, Gruzdev A, Seidel L, Bengsch B, Shears SB, *et al.*2023. Capillary electrophoresis mass spectrometry identifies new isomers of inositol pyrophosphates in mammalian tissues. *Chemical Science* **14**: 658–667.
Qiu D, Wilson MS, Eisenbeis VB, Harmel RK, Riemer E, Haas TM, Wittwer C, Jork N, Gu C, Shears SB, *et al.*2020. Analysis of inositol phosphate metabolism by capillary electrophoresis electrospray ionization mass spectrometry. *Nature Communications* **11**: 6035.
R Core Team. **2023**. R: A language and environment for statistical computing.
Rappsilber J, Ishihama Y, Mann M. **2003**. Stop and Go Extraction Tips for Matrix-Assisted Laser Desorption/Ionization, Nanoelectrospray, and LC/MS Sample Pretreatment in Proteomics. *Analytical Chemistry* **75**: 663–670.
Ried MK, Wild R, Zhu J, Pipercevic J, Sturm K, Broger L, Harmel RK, Abriata LA, Hothorn LA, Fiedler D, *et al.*2021. Inositol pyrophosphates promote the interaction of SPX domains with the coiled-coil motif of PHR transcription factors to regulate plant phosphate homeostasis. *Nature Communications* **12**: 384.
Riemer E, Qiu D, Laha D, Harmel RK, Gaugler P, Gaugler V, Frei M, Hajirezaei M-R, Laha NP, Krusenbaum L, *et al.*2021. ITPK1 is an InsP6/ADP phosphotransferase that controls phosphate signaling in Arabidopsis. *Molecular Plant* **14**: 1864–1880.
Ritter K, Jork N, Unmüßig A-S, Köhn M, Jessen HJ. **2023**. Assigning the Absolute Configuration of Inositol Poly- and Pyrophosphates by NMR Using a Single Chiral Solvating Agent. *Biomolecules* **13**: 1150.
Rubio V, Linhares F, Solano R, Martín AC, Iglesias J, Leyva A, Paz-Ares J. **2001**. A conserved MYB transcription factor involved in phosphate starvation signaling both in vascular plants and in unicellular algae. *Genes & Development* **15**: 2122–2133.
Safrany ST, Caffrey JJ, Yang X, Bembenek ME, Moyer MB, Burkhart WA, Shears SB. **1998**. A novel context for the 'MutT' module, a guardian of cell integrity, in a diphosphoinositol polyphosphate phosphohydrolase. *The EMBO Journal* **17**: 6599–6607.
Safrany ST, Ingram SW, Cartwright JL, Falck JR, McLennan AG, Barnes LD, Shears SB. **1999**. The Diadenosine Hexaphosphate Hydrolases fromSchizosaccharomyces pombe and Saccharomyces cerevisiae Are Homologues of the Human Diphosphoinositol Polyphosphate Phosphohydrolase: OVERLAPPING SUBSTRATE SPECIFICITIES IN A MutT-TYPE PROTEIN *. *Journal of Biological Chemistry* **274**: 21735–21740.
Saiardi A, Erdjument-Bromage H, Snowman AM, Tempst P, Snyder SH. **1999**. Synthesis

of diphosphoinositol pentakisphosphate by a newly identified family of higher inositol polyphosphate kinases. *Current Biology* **9**: 1323–1326.
Shears SB. **2015**. Inositol pyrophosphates: why so many phosphates? *Advances in Biological Regulation* **57**: 203–216.
Shears SB. **2018**. Intimate connections: Inositol pyrophosphates at the interface of metabolic regulation and cell signaling. *Journal of Cellular Physiology* **233**: 1897–1912.
Shi J, Hu H, Zhang K, Zhang W, Yu Y, Wu Z, Wu P. **2014**. The paralogous SPX3 and SPX5 genes redundantly modulate Pi homeostasis in rice. *Journal of Experimental Botany* **65**: 859–870.
Steidle EA, Chong LS, Wu M, Crooke E, Fiedler D, Resnick AC, Rolfes RJ. **2016**. A Novel Inositol Pyrophosphate Phosphatase in Saccharomyces cerevisiae: Siw14 PROTEIN SELECTIVELY CLEAVES THE β-PHOSPHATE FROM 5-DIPHOSPHOINOSITOL PENTAKISPHOSPHATE (5PP-IP5) *. *Journal of Biological Chemistry* **291**: 6772–6783.
Stephens L, Radenberg T, Thiel U, Vogel G, Khoo KH, Dell A, Jackson TR, Hawkins PT, Mayr GW. **1993**. The detection, purification, structural characterization, and metabolism of diphosphoinositol pentakisphosphate(s) and bisdiphosphoinositol tetrakisphosphate(s). *Journal of Biological Chemistry* **268**: 4009–4015.
Stevenson-Paulik J, Bastidas RJ, Chiou S-T, Frye RA, York JD. **2005**. Generation of phytate-free seeds in Arabidopsis through disruption of inositol polyphosphate kinases. *Proceedings of the National Academy of Sciences* **102**: 12612–12617.
Stevenson-Paulik J, Odom AR, York JD. **2002**. Molecular and biochemical characterization of two plant inositol polyphosphate 6-/3-/5-kinases. *The Journal of Biological Chemistry* **277**: 42711–42718.
Storey J, Bass A, Dabney A, Robinson D, Warnes G. **2024**. qvalue: Q-value estimation for false discovery rate control. *Bioconductor*.
Sweetman D, Stavridou I, Johnson S, Green P, Caddick SEK, Brearley CA. **2007**. Arabidopsis thaliana inositol 1,3,4-trisphosphate 5/6-kinase 4 (AtITPK4) is an outlier to a family of ATP-grasp fold proteins from Arabidopsis. *FEBS Letters* **581**: 4165–4171.
Szijgyarto Z, Garedew A, Azevedo C, Saiardi A. **2011**. Influence of inositol pyrophosphates on cellular energy dynamics. *Science (New York, N.Y.)* **334**: 802–805.
Tanaka H, Maruta T, Ogawa T, Tanabe N, Tamoi M, Yoshimura K, Shigeoka S. **2015**. Identification and characterization of Arabidopsis AtNUDX9 as a GDP-d-mannose pyrophosphohydrolase: its involvement in root growth inhibition in response to ammonium. *Journal of Experimental Botany* **66**: 5797–5808.
Thota SG, Bhandari R. **2015**. The emerging roles of inositol pyrophosphates in eukaryotic cell physiology. *Journal of Biosciences* **40**: 593–605.
Tilman D, Cassman KG, Matson PA, Naylor R, Polasky S. **2002**. Agricultural sustainability and intensive production practices. *Nature* **418**: 671–677.
Tyanova S, Temu T, Cox J. **2016**. The MaxQuant computational platform for mass spectrometry-based shotgun proteomics. *Nature Protocols* **11**: 2301–2319.
Ursache R, Fujita S, Dénervaud Tendon V, Geldner N. **2021**. Combined fluorescent seed selection and multiplex CRISPR/Cas9 assembly for fast generation of multiple Arabidopsis mutants. *Plant Methods* **17**: 111.
Wang H, Falck JR, Hall TMT, Shears SB. **2011**. Structural basis for an inositol pyrophosphate kinase surmounting phosphate crowding. *Nature chemical biology* **8**: 111–116.
Wang L, Feng Z, Wang X, Wang X, Zhang X. **2010**. DEGseq: an R package for identifying differentially expressed genes from RNA-seq data. *Bioinformatics (Oxford, England)* **26**: 136–138.
Wang H, Gu C, Rolfes RJ, Jessen HJ, Shears SB. **2018**. Structural and biochemical characterization of Siw14: A protein-tyrosine phosphatase fold that metabolizes inositol pyrophosphates. *The Journal of Biological Chemistry* **293**: 6905–6914.
Wang Z, Kuo H-F, Chiou T-J. **2021**. Intracellular phosphate sensing and regulation of phosphate transport systems in plants. *Plant Physiology* **187**: 2043–2055.
Wang H, Nair VS, Holland AA, Capolicchio S, Jessen HJ, Johnson MK, Shears SB.

2015. Asp1 from Schizosaccharomyces pombe binds a [2Fe-2S](2+) cluster which inhibits inositol pyrophosphate 1-phosphatase activity. *Biochemistry* **54**: 6462–6474.
Wang H, Perera L, Jork N, Zong G, Riley AM, Potter BVL, Jessen HJ, Shears SB. **2022**. A structural exposé of noncanonical molecular reactivity within the protein tyrosine phosphatase WPD loop. *Nature Communications* **13**: 2231.
Wang Z, Ruan W, Shi J, Zhang L, Xiang D, Yang C, Li C, Wu Z, Liu Y, Yu Y, *et al.*2014. Rice SPX1 and SPX2 inhibit phosphate starvation responses through interacting with PHR2 in a phosphate-dependent manner. *Proceedings of the National Academy of Sciences of the United States of America* **111**: 14953–14958.
Whitfield HL, Rodriguez RF, Shipton ML, Li AWH, Riley AM, Potter BVL, Hemmings AM, Brearley CA. **2024**. Crystal Structure and Enzymology of Solanum tuberosum Inositol Tris/Tetrakisphosphate Kinase 1 (StITPK1). *Biochemistry* **63**: 42–52.
Whitfield H, White G, Sprigg C, Riley AM, Potter BVL, Hemmings AM, Brearley CA. **2020**. An ATP-responsive metabolic cassette comprised of inositol tris/tetrakisphosphate kinase 1 (ITPK1) and inositol pentakisphosphate 2-kinase (IPK1) buffers diphosphosphoinositol phosphate levels. *Biochemical Journal* **477**: 2621–2638.
Wickham H, Averick M, Bryan J, Chang W, McGowan LD, François R, Grolemund G, Hayes A, Henry L, Hester J, *et al.*2019. Welcome to the Tidyverse. *Journal of Open Source Software* **4**: 1686.
Wickham H, François R, Henry L, Müller K, Vaughan D, Software P, PBC. **2023**. dplyr: A Grammar of Data Manipulation.
Wild R, Gerasimaite R, Jung J-Y, Truffault V, Pavlovic I, Schmidt A, Saiardi A, Jessen HJ, Poirier Y, Hothorn M, *et al.*2016. Control of eukaryotic phosphate homeostasis by inositol polyphosphate sensor domains. *Science (New York, N.Y.)* **352**: 986–990.
Wilke CO. **2024**. cowplot: Streamlined Plot Theme and Plot Annotations for ‘ggplot2’.
Wilson MSC, Bulley SJ, Pisani F, Irvine RF, Saiardi A. **2015**. A novel method for the purification of inositol phosphates from biological samples reveals that no phytate is present in human plasma or urine. *Open Biology* **5**: 150014.
Wilson MS, Jessen HJ, Saiardi A. **2019**. The inositol hexakisphosphate kinases IP6K1 and -2 regulate human cellular phosphate homeostasis, including XPR1-mediated phosphate export. *The Journal of Biological Chemistry* **294**: 11597–11608.
Wu M, Chong LS, Perlman DH, Resnick AC, Fiedler D. **2016**. Inositol polyphosphates intersect with signaling and metabolic networks via two distinct mechanisms. *Proceedings of the National Academy of Sciences of the United States of America* **113**: E6757–E6765.
Xia H-J, Brearley C, Elge S, Kaplan B, Fromm H, Mueller-Roeber B. **2003**. Arabidopsis Inositol Polyphosphate 6-/3-Kinase Is a Nuclear Protein That Complements a Yeast Mutant Lacking a Functional ArgR-Mcm1 Transcription Complex. *The Plant Cell* **15**: 449–463.
Xu J, Yang J-Y, Niu Q-W, Chua N-H. **2006**. Arabidopsis DCP2, DCP1, and VARICOSE Form a Decapping Complex Required for Postembryonic Development. *The Plant Cell* **18**: 3386–3398.
Yadav R, Liu G, Rana P, Pullagurla NJ, Qiu D, Jessen HJ, Laha D. **2023**. Conservation of heat stress acclimation by the inositol polyphosphate multikinase, IPMK responsible for 4/6-InsP7 production in land plants. : 2023.11.17.567642.
Yan R, Chen H, Liu C, Zhao J, Wu D, Jiang J, Gong J, Jiang D. **2024**. Human XPR1 structures reveal phosphate export mechanism. *Nature* **633**: 960–967.
Yoshimura K, Ogawa T, Ueda Y, Shigeoka S. **2007**. AtNUDX1, an 8-Oxo-7,8-Dihydro-2′-Deoxyguanosine 5′-Triphosphate Pyrophosphohydrolase, is Responsible for Eliminating Oxidized Nucleotides in Arabidopsis. *Plant and Cell Physiology* **48**: 1438–1449.
Yoshimura K, Shigeoka S. **2015**. Versatile physiological functions of the Nudix hydrolase family in Arabidopsis. *Bioscience, Biotechnology, and Biochemistry* **79**: 354–366.
Zhong Y, Wang Y, Guo J, Zhu X, Shi J, He Q, Liu Y, Wu Y, Zhang L, Lv Q, *et al.*2018. Rice SPX6 negatively regulates the phosphate starvation response through suppression of the transcription factor PHR2. *The New Phytologist* **219**: 135–148.
Zhu J, Lau K, Puschmann R, Harmel RK, Zhang Y, Pries V, Gaugler P, Broger L, Dutta AK, Jessen HJ, *et al.*2019. Two bifunctional inositol pyrophosphate kinases/phosphatases

control plant phosphate homeostasis. *eLife* **8**: e43582.